Title
The Electrodeposition of Iron Phosphide Film for Efficient Hydrogen Evolution Reaction

Author
Lu, Zhipeng

Publication Date
2020

Peer reviewed|Thesis/dissertation

UNIVERSITY OF CALIFORNIA

Santa Barbara

The Electrodeposition of Iron Phosphide Film for Efficient Hydrogen Evolution Reaction

A Thesis submitted in partial satisfaction of the

requirements for the degree Master of Science

in Chemistry

by

Zhipeng Lu

Committee in charge:

Professor Lior Sepunaru, Chair

Professor Javier Read de Alaniz

Professor Armen Zakarian

Professor Mattanjah S. de Vries

September 2020

The thesis of Zhipeng Lu is approved.

_____

Javier Read de Alaniz

_____

Armen Zakarian

_____

Mattanjah S. de Vries

_____

Lior Sepunaru, Committee Chair

September 2020

The Electrodeposition of Iron Phosphide Film for Efficient Hydrogen Evolution Reaction

ACKNOWLEDGEMENTS

I would like to thank Department of Chemistry and Biochemistry at UCSB for granting me an offer. It turns out be a great place for study, research and living.

I very much appreciate my mentor Dr. Sepunaru for his financial and academic supports on me. Dr. Sepunaru, the greatest mentor in the world, who taught me not only how to do scientific research but also how to become a caring person. Without him, I won't be able to peruse my academic dream.

I am also grateful to my committee member for their help on improving this thesis's quality. Thank you, Dr. Javier Read de Alaniz, Dr. Armen Zakarian and Dr. Mattanjah S. de Vries.

I would like to acknowledge Aidan Taylor, Claire Chisholm, Tom Mates, Weiwei Li and Guang Wu for their technical help on the characterizations of FeP film.

I would like to thank my groupmates Connor Davis, Julia Chung, Stephanie Wang, Brian Roehrich and Arunavo Chakraborty for the inspiration on chemistry and enjoyable coffee/beer times.

At last, I would like to express my great gratitude to my parents, my brother and my girlfriend Chuanxiuyue He. Their unconditional support is of great importance to me. It is the ultimate source of strength to me.

ABSTRACT

The Electrodeposition of Iron Phosphide Film for Efficient Hydrogen Evolution Reaction

by

Zhipeng Lu

The rapidly developing world poses a high energy demand. Hydrogen is recognized as one of the most important renewable energy sources with some great features including cleanness, and high gravimetric energy density. Hydrogen is predominantly produced by steam-methane reforming process at present, which is an energy intensive and CO_2 emission intensive process. Alternatively, the hydrogen evolution reaction (HER) by electrochemical water splitting is part of a sustainable and scalable process to produce H_2. Currently, precious metal platinum is required to catalyze this reaction which limits its industrial application. Hence, the design of a highly efficient and low-cost electrocatalyst is in demand. Recently, metal phosphides were developed as a good substitute of platinum for HER catalysis. Some examples are nickel phosphide, cobalt phosphide, iron phosphide. All of them have shown excellent HER activity and stability. Among them, iron phosphide is particularly attractive because of the abundance of iron on earth. Traditionally, the synthesis of iron phosphide is based on high temperature process that generates highly corrosive and flammable phosphine byproduct. Thus, greener and more straightforward synthetic method is desired. Herein, an easy and cost-effective method is developed to electrodeposit iron phosphide (FeP) film on a copper electrode at room temperature. The pulsed electrodeposition method was used to electrochemically etch co-deposited metallic iron which improved the film's stability. In addition, formic acid and pH are crucial to promoting FeP deposition and it was well explained by experiments of cyclic voltammetry, capacitance studies, electron microscopy, and inductively coupled plasma mass spectrometry.

The as-deposited FeP film was shown to be a highly active HER catalyst in all-pH conditions. The FeP modified electrode produced current densities of-10 mA/cm^2 at a low overpotential of 66 mV in 0.5 M sulfuric acid (H_2SO_4, pH=0.3), 131 mV in 1.0 M phosphate buffer (PB, pH=6.4), and 110 mV in 1.0 M potassium hydroxide (KOH, pH=14.0) solution, as well as a Tafel slope of 55 mV/dec, 108 mV/dec, 60 mV/dec, respectively. Electrochemical impedance studies revealed the low charge transfer resistance and fast HER kinetics of FeP electrocatalyst. More importantly, the film has excellent stability during HER catalysis under acidic and neutral conditions, as shown by long-term chronoamperometry, supported further with electron microscopy, and X-ray photoelectron spectroscopy. Specifically, the overpotentials increased diminutively 7 mV after 24 hours of electrocatalysis at a current density of -10 mA/cm^2 in acidic solution. Similarly, only a 10 mV increase in overpotential was observed under neutral conditions. Overall, in this work, I was able to successfully demonstrate that a carefully controlled electrodeposition process provided a simple yet powerful method to synthesize heterogeneous iron phosphide catalyst that is highly efficient towards hydrogen evolution reaction. Via potentiostatic tuning of the deposition rate proceeding by electrochemical etching of phosphide reach inactive alloy, we were able to achieve a 2-D film that could find applications in large scale hydrogen production under wide range of industrial conditions.

TABLE OF CONTENTS

Chapter 1. Introduction

Energy is of great importance to human civilization. Expectedly, the world energy consumption increases year by year. The search for abundant, clean, and cheap energy supply has been the research focus of numerous scientists over decades.[1,2] Currently, fossil fuel is still the largest energy source. Although it is a reliable energy source, it causes many problems such as air pollutions and global warming mostly via CO_2 emission. More importantly, it cannot be easily regenerated thus not sustainable. In contrast, renewable energy sources include solar power, wind power, hydropower, biomass, geothermal power are much favorable due to its cleanness and abundance and broad geographic distribution. In addition, renewable energy can be coupled with chemistry and chemical engineering to generate high value-added products.

1.1. Hydrogen Energy

Hydrogen is a non-natural available but renewable resource than can be produced in a completely sustainable way.[3] Hydrogen energy is a promising energy supply with various advantages. First, it has an extremely high gravimetric energy density of 143 MJ kg^{-1} which is three times higher than liquid gasoline.[4] Second, it can be produced virtually any place in the world because of the precursor's abundance. Third, it is clean energy with the nonharmful water as the only combustion product. Fourth, renewable energy can be used for its production. At last, it is an excellent energy carrier for storage to utilize those surplus energy generated by power plants. Although hydrogen energy is sometimes criticized because of the challenge in storage and transportation,[5] it is still an appealing energy source considering all the advantages stated previously.

1.2. Hydrogen production

Hydrogen can be produced from fossil fuels and water. At present, the steam methane reforming process and water-gas shift reaction are the dominant way for hydrogen production because of its low cost and because the production process was perfected over the years to exploit maximum efficiency.[6] As shown in Scheme 1, this process is highly energy-intensive which requires 700 to 1000 °C and a metal catalyst. Besides, it generates a tremendous amount of CO_2 as the byproduct. Even more, the precursor for this process natural gas is not a renewable source.

Steam reforming

$$CH_4 + H_2O \rightleftharpoons CO + 3\,H_2$$

Wster-gas shift reaction

$$CO + H_2O \rightleftharpoons CO_2 + H_2$$

Scheme 1. Steam reforming process and waster-gas shift reaction.

Alternatively, hydrogen production by electrochemical water splitting can operate under milder conditions (room temperature) with easily available water precursor.[7–11] The half-reaction cathodic process of water electrolysis is named hydrogen evolution reaction (HER). As shown in Figure 1, HER has an activation energy barrier which is represented as overpotential, η. The overpotential which is defined as the difference between the equilibrium potential and applied potential directly relates to the energy efficiency of electrolysis. Therefore, the research on efficient, cost effective HER electrocatalyst with low overpotential is in high demand.

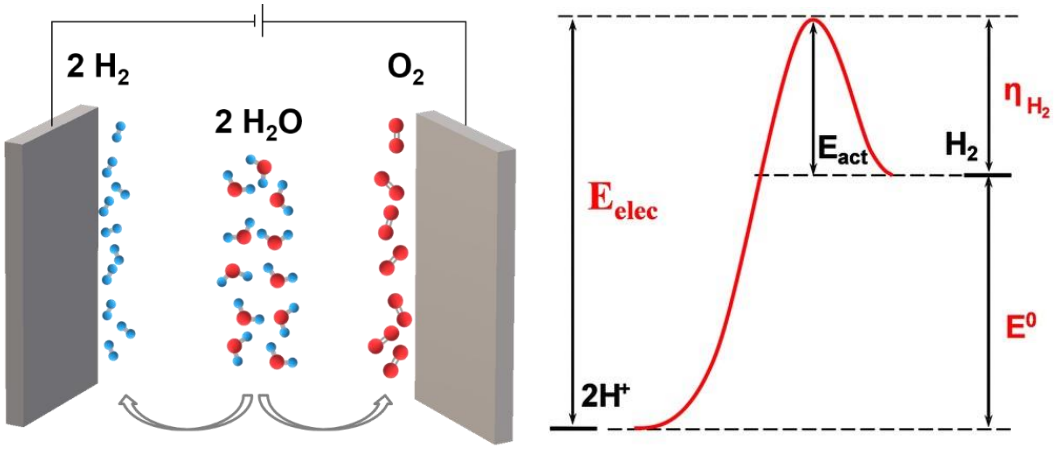

Figure 1. LEFT: Electrochemical water splitting. Water is electrolyzed into hydrogen and oxygen; RIGHT: the thermodynamics of HER which shows the relationship between applied electrode potential E_{elec}, thermmodynamic equilibrium potential E^0 and overpotential η_{H_2}. Reproduced from Ref. 10 with permission from The Royal Society of Chemistry.

At present, platinum derived electrocatalysts are the state-of-the-art, although its industrial application is limited by its scarcity and high cost; thus, it is urgent to utilize earth-abundant materials as a substitute for platinum. Many non-noble metal compounds such as phosphide,[12–14] chalcogenide,[15,16], and carbides[17] have shown rather competitive catalytic performance as well as good stability for HER. In particular, iron phosphide (FeP) is highlighted because of its abundance and hence potential cost efficiency. Hitherto, several approaches have been demonstrated for the successful synthesis of iron phosphide and can be categorized as either a solution-phase reaction between organic iron precursor and tri-n-octylphosphine[18,19] or a gas-solid reaction named phosphorization.[20–22] Although high-quality and even crystalline FeP materials can be obtained, these methods require high temperatures (ranging from 300-400 ℃) and may generate highly corrosive and flammable phosphine (PH_3) as a byproduct resulting from the decomposition of a phosphide precursor. As a comparison,

electrodeposition offers an alternative synthetic route, featuring mild and electrochemically controlled experimental conditions, high-cost efficiency, easy set-up, and facile scale-up. In addition, this process is binder-free so that the catalyst is directly deposited on the electrode without drop casting steps to avoid material loss. The first report of direct electrodeposition of FeP film for HER applications was published by Sequeria et al.[23] In their work, the as-deposited iron phosphide generated under galvanostatic conditions was considerably iron-rich ($Fe_{87}P_{13}$) and relatively inefficient for HER (>350 mV at -10 mA/cm^2 in 1.0 M NaOH). Very recently, Zhang-hui et al. used the similar electrodeposition strategy but with acid-etching to increase P to Fe ratio. With that, they were able to produce FeP film with better HER activity (η_{-10mA/cm^2} =140 mV in 1.0 M KOH and η_{-10mA/cm^2} =110 mV in 0.5 M H_2SO_4).[24]

Herein, we report a straightforward and cost-effective approach to prepare an iron phosphide film by electrodeposition under potentiostatic conditions. Instead of acid-etching, we applied pulsed electrodeposition strategy which simplified the procedure. More importantly, the as-prepared iron phosphide film has completely different morphology and much better catalytic activity for the HER at full pH range (0-14), which demonstrates its potential application in proton exchange membrane electrolysis (acid media),[25] microbial electrolysis cell (neutral media)[26] and industrial water electrolysis (basic media).[27]

Chapter 2. Experimental Methods

2.1. Materials

2.1.1. Electrode Materials

Copper foil (0.25 mm thick, 99.98%) were purchased from Sigma Aldrich. Graphite rod electrode (99.9995%) were purchased from Alfa Aesar. Platinum wire, saturated calomel electrode (SCE) were purchased from CH Instruments, Inc. Reversible hydrogen electrode Hydroflex® electrode was purchased from Gaskatel.

2.1.2. Chemical Agents

Sulfuric acid (99.999%), sodium phosphate dibasic (Na_2HPO_4, ⩾ 99%), sodium phosphate monobasic (NaH_2PO_4, ⩾99%) and potassium hydroxide (KOH, ⩾85%) were purchased from Sigma Aldrich. Ferrous sulfate heptahydrate ($FeSO_4 \cdot 7H_2O$, certified ACS grade) and formic acid (HCOOH, 99%) were purchased from Fisher. Sodium hypophosphite (NaH_2PO_2) was purchased from Riedelde Haën. Platinum on carbon black (20% Pt/C, HiSPEC® 3000), Nafion® D-520 (5% wt. in water and 1-propanol mixture) and graphite rod electrode (99.9995%) were purchased from Alfa Aesar. High-quality colloidal Ag paint was purchased from SPI Supplies, and two-part epoxy [HYSOL 9460] was purchased from McMaster-Carr. All chemicals were used as received without further purification and all aqueous solutions were prepared with ultrapure water (>18.2 MΩ.cm) obtained from Labconco® water purification system.

2.2. Electrode Preparation

2.2.1. Fabrication of Copper Foil Electrode

A small piece of copper foil was connected to a polyvinylchloride PVC-coated Cu wire using Ag paint. Then, the junction point and the copper foil were insulated with two-part epoxy except 0.2 cm^2 [0.2 cm×0.5 cm × 2 (double sided)] of copper that was left exposed and defined the electrode surface area.

2.2.2. Fabrication of Pt/C Electrode

2 mg 20% Pt/C and 17.5 µl 5% Nafion were dispersed in 500 µl EtOH and sonicated for 15 min to form a homogeneous solution. A 129.4 µl solution was drop casted on the Cu electrode and then dried in air at room temperature. The mass loading of Pt was 0.5 mg cm^{-2}.

2.2.3. Electrodeposition of FeP Film

Copper foil electrode was used as the substrate electrode for iron phosphide film electrodeposition. Before electrodeposition, the copper foil was immersed in 1.0 M HCl for 5 min to remove surface oxide layer, then washed with ultrapure water and acetone several times, and finally dried in N_2 flow. The deposition electrolytes solution was obtained by dissolving 5.0 g $FeSO_4 \cdot 7H_2O$ (0.72 M), 1.58 g NaH_2PO_2 (0.72 M) and 0.25 ml of formic acid (1 vol. %) in ultrapure water to reach a final volume of 25 ml. The pH was adjusted to 1.5 by adding sulfuric acid slowly and was measured by Accumet AB150 pH meter. Electrodeposition was performed using a standard three-electrode system. Copper foil, platinum wire, saturated calomel electrode (SCE) were used as working electrode, counter electrode and reference

electrode, respectively. The deposition potential was held at -1.7 V for 120 s, then immediately switched into -0.1 V for 240 s to remove excessively co-deposited metallic iron. These two steps were repeated seven more times to increase the thickness of film. Finally, a black FeP film was observed as a deposit on the copper foil and later rinsed with ultrapure water carefully and dried in air for further use. The mass loading is calculated as 2.6 mg/cm^2 based on the mass difference before and after electrodeposition. Pictures of electrodeposition set-up, as-deposited FeP electrode (Figure 2) and electrodeposition current-time profile (Figure 3) can be found below. All measurements were done at 25 ℃.

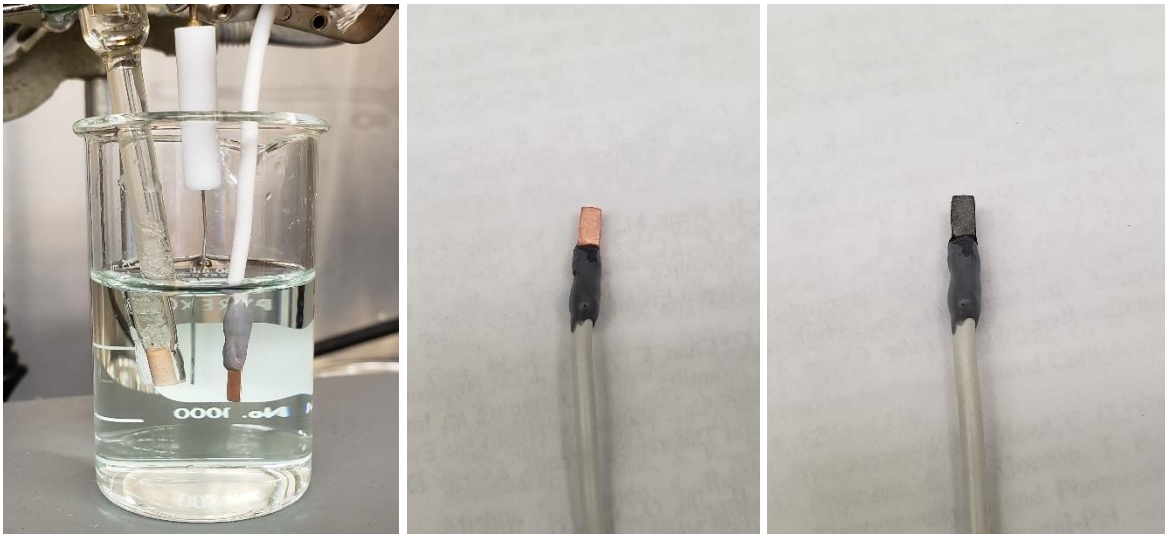

Figure 2. Electrochemical deposition set-up (LEFT); Copper foil electrode before electrodeposition (MIDDLE); As-deposited FeP electrode (RIGHT).

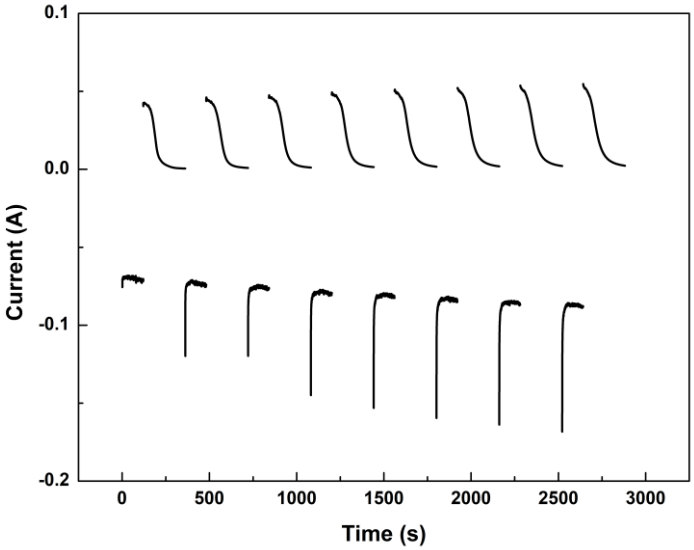

Figure 3. Electrodeposition current-time profile.

2.3. Characterizations

2.3.1. Electrochemical Characterization

Unless specified, electrochemical measurements were performed on an Autolab M204 electrochemical workstation. Linear sweep voltammetry was performed with a three-electrode system configuration using a graphite rod and a Hydroflex® electrode as counter electrode and reference electrode, respectively. In addition, LSV were recorded at a scan rate of 2 mV/s to minimize capacitive current and was repeated multiple times until stable data were acquired. All LSV curves were IR-compensated and the current-interrupt method was used to measure uncompensated resistance (3 Ω in 0.5 M H_2SO_4 and 1.0 M KOH solution, 10 Ω in 1.0 M phosphate buffer).

The electrochemical stability was evaluated using chronoamperometry with graphite rod electrode and SCE as counter and reference electrode, respectively. Specifically, a constant

current density of -10 mA cm^{-2} was applied for 24 h and the corresponding potential was recorded. The change in the overpotential demonstrated the stability of FeP film during HER.

Electrochemical impedance spectra (EIS) were measured on Biologic SP-300 potential stats at an overpotential of 100 mV (vs RHE) in the frequency range of 0.01Hz – 100 kHz using a 5 mV amplitude AC signal. A graphite rod and a Hydroflex® electrode were used as counter electrode and reference electrode, respectively. The simulation of results by electrical equivalent circuit was done on EC-Lab® software.

Cyclic voltammetry (CV) were performed to study electrodeposition mechanism and electrochemical active surface area. For electrodeposition mechanism study, it was recorded at a scan rate of 100 mV/s in the solutions of 0.72 M $FeSO_4$, 0.72 M NaH_2PO_2, 0.72 M $FeSO_4$+0.72 M NaH_2PO_2, 0.72 M $FeSO_4$+0.72 M NaH_2PO_2+1 vol% HCOOH at pH=1.5, respectively. The applied potential range was 0.0 – 2.0 V vs SCE. For electrochemical active surface area study, it was recorded at various scan rate with a potential range of 0 – 150 mV vs RHE in 0.5 M H_2SO_4 solution. The capacitive current at 75 mV vs RHE was used to calculate the electrode's capacitance.

Faradaic efficiencies (FE) were evaluated using a three-electrode system. Graphite electro de and SCE electrode were used as counter and reference electrode, respectively. An inverted graduated cylinder filled with electrolyte solution was positioned above FeP electrode to collect H_2 bubbles generated by electrolysis. A cathodic current of 10 mA was applied into the 0.2 cm^2 working electrode until 40 coulombs of charge passed.

All measurements were done at 25 ℃.

2.3.2. Electron Microscopic/Spectroscopic Characterization

Scanning electron microscopy (SEM) images were collected using Thermo Scientific™ Apreo SEM at an accelerating voltage of 10.00 kV, at a working distance of 9.3 mm and at a beam current of 1.6 nA. Energy dispersive X-ray spectroscopy (EDX) data and elemental mapping data were collected at an accelerating voltage of 20.00 kV. X-ray photoelectron spectroscopy (XPS) data were collected using a Kratos Axis Ultra DLD system (Kra-tos Analytical, Manchester, UK). The input X-rays were mono-chromated Al k-alpha (1486 eV) operating at 168 W. Survey data were taken at a pass energy of 160 eV (500 meV channel width), and high-resolution data at 20 eV (50 meV). Transmission electron spectroscopy (TEM) images were collected at Thermo Scientific™ Talos G2 at an accelerating voltage of 200 kV. TEM samples were dispersed in ethanol (0.05 mg/ml) and sonicated for 30 min. Then, it was drop casted onto lacey carbon film 300 mesh Cu grids (Ted Pella) and air dried.

2.3.3. Other Characterization (XRD, ICP-MS)

X-ray diffraction (XRD) were done using Bruker Proteum system with Proteum CCD detector and Cu-K-alpha radiation source from MicroStar rotating anode.

Inductively coupled plasma mass spectrometry (ICP-MS) was performed on Agilent 7900 ICP-MS instruments to determine the elemental ratio of Fe to P. The electrochemical deposited FeP films were scratched from electrode then they were digested in aqua regia and diluted with ultrapure water. The final concentration of acid was 2%. A series of external standards with different concentrations were used for calibration.

Chapter 3. Results and Discussions

3.1. The Electrodeposition Mechanism

The possible mechanism of FeP electrochemical deposition was shown in Scheme 2. [28,29]

$$H_2PO_2^- + 5\,H^+ + 4\,e^- = PH_3 + 2\,H_2O \quad (1)$$

$$2\,PH_3 + 3\,Fe^{2+} = 3\,Fe + 2\,P + 6\,H^+ \quad (2)$$

$$Fe^{2+} + 2\,e^- = Fe\ (metallic) \quad (3)$$

Scheme 2. Possible mechanism of FeP electrodeposition.

3.2. The Characterization of As-deposited FeP film

The as-deposited FeP film was characterized by SEM, EDX, TEM, XRD, XPS and ICP-MS. First, the ratio of Fe to P was determined to be 1.03 by ICP-MS, thus confirming the composition of FeP film. As seen in Figure 4, scanning electron microscopy image of the as-deposited film showed that its film morphology resembled cracked clays. It leaded to a higher surface area compared to an uncracked film. The electrochemical etching of co-deposited metallic iron will leave vacant sites which might explain the formation of valleys. Energy dispersive X-ray spectroscopy (EDX) mapping was applied to demonstrate the spatial distribution of element iron and phosphorous. As shown in Figure 4, the surface of those plateaus was majorly composed of iron and phosphorous and the distribution was even. It confirmed the chemical nature of FeP film. Meanwhile, some copper was founded at the bottom of valley. Those signals should origin from the copper foil electrodes.

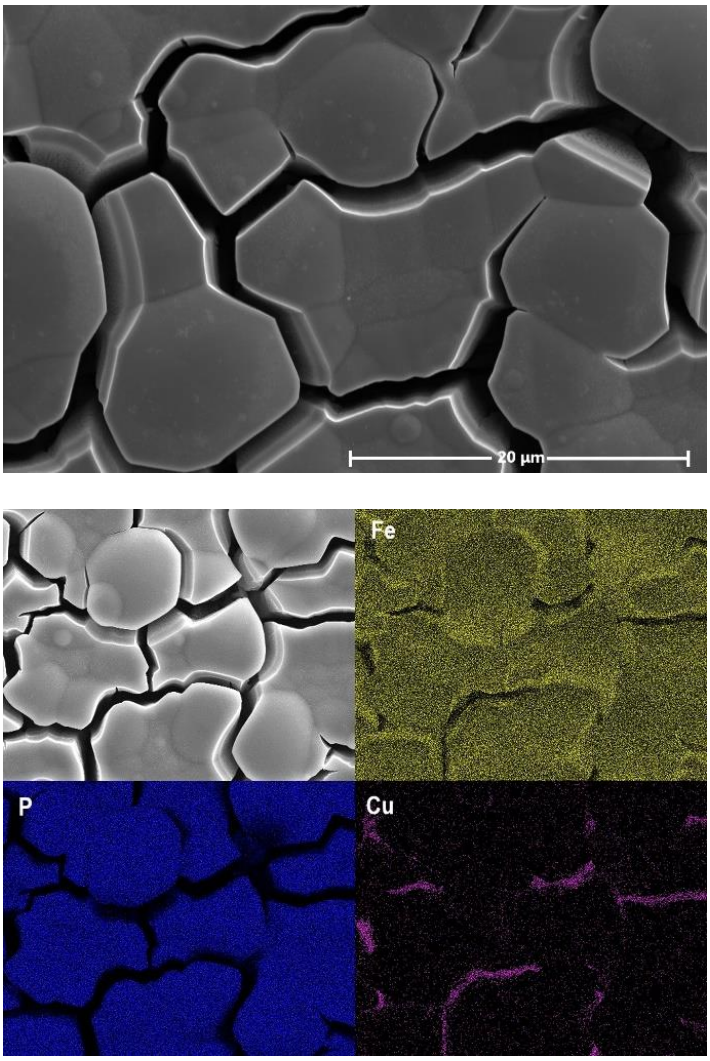

Figure 4. SEM images (TOP) and EDX mapping (BOTTOM) of as-deposited FeP film.

To further investigate the chemical structure of the FeP film, X-ray photoelectron spectroscopy analysis was performed on the as-deposited electrodes. The Fe 2p spectrum was shown in Figure 5. Two predominant peaks at 707.1 eV and 720.1 eV were assigned to Fe 2p doublet indicative of Fe^{3+} in FeP, while the small peak at 710.5 eV as well as the small, broad peak at 724.0 eV were ascribed to the 2p 3/2 and 2p 1/2 of Fe^{3+} in oxidized Fe species arising from surface oxidation.[21,22] In the P 2p region, the doublet at 129.3 eV and 130.1 eV indicated

phosphide bonded to iron. The peak at 132.9 eV was identified as P in the phosphate (PO_4^{3-}).[21,22] Overall, XPS demonstrated the identify of iron phosphide film.

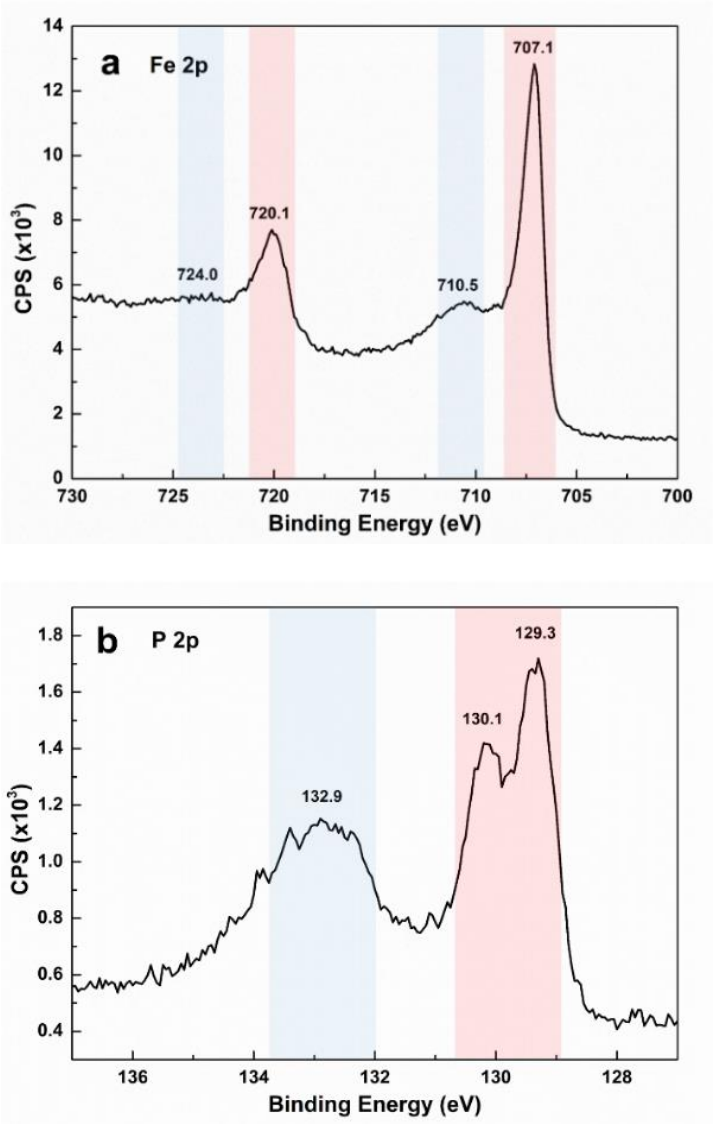

Figure 5. XPS of as-deposited FeP film, (a) Fe 2p band (b) P 2p band. Notes: red column (FeP), blue column (oxidized Fe or P species), CPS: counts per second.

To understand the crystallinity of electrodeposited FeP material, transmission electron microscopy was used for characterization. As Figure 6 shown, no crystal lattice was observed. Based on the selected area electron diffraction, our material revealed the characteristic halo

ring pattern of amorphous material. The amorphous properties of FeP were further confirmed by the X ray diffraction (Figure 7). Only peaks from copper substrate were found and no crystalline FeP peaks were found.

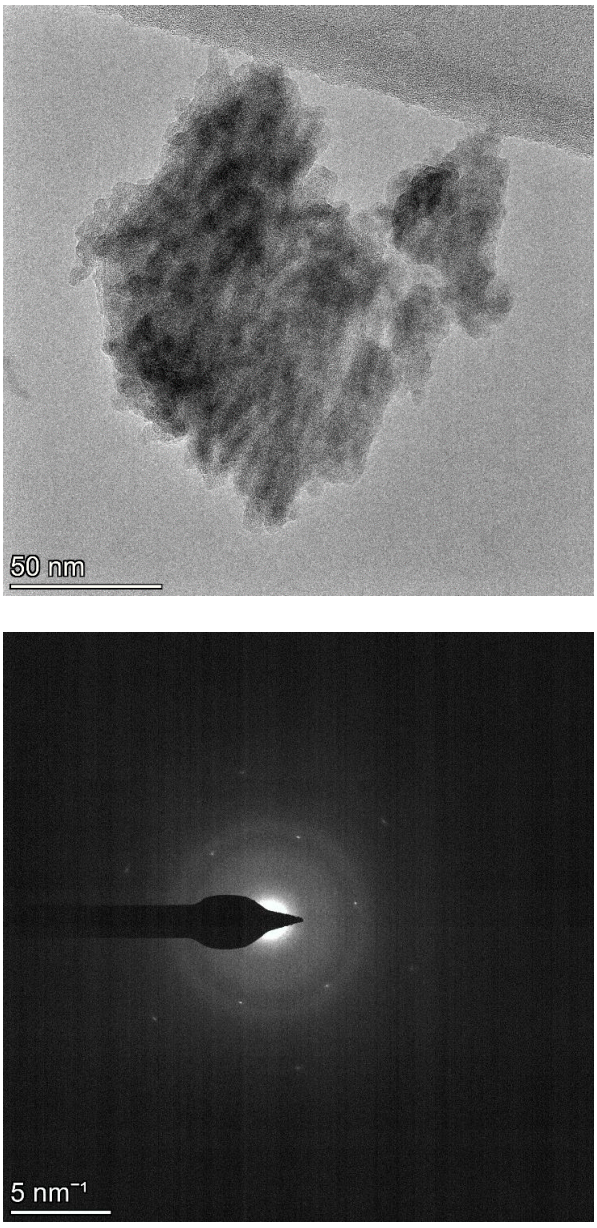

Figure 6. TEM (LEFT) image and SAED pattern of FeP material. (Note: The diffraction spots in SAED came from the carbon membrane of the TEM grid but not from FeP.)

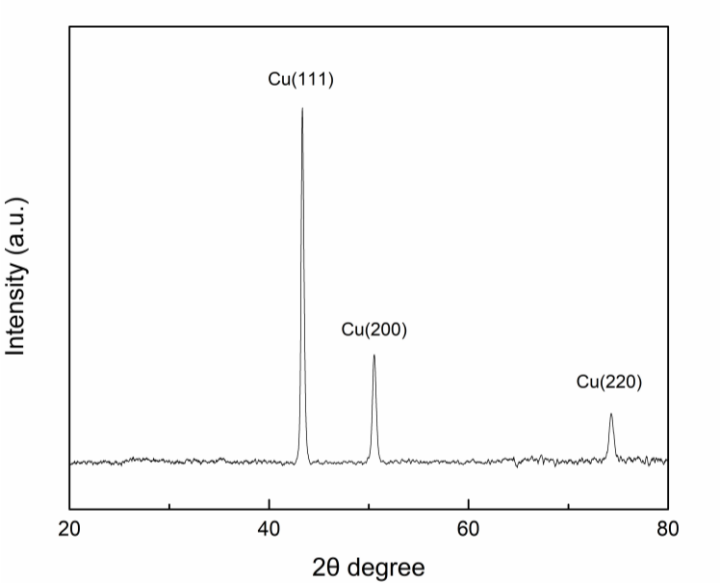

Figure 7. XRD spectrum of as-deposited FeP film. Note: XRD curve was shown after background subtraction.

3.3. Electrochemical HER activity

3.3.1 The Optimization Process

Three parameters were investigated during the optimization process: 1). Deposition time; 2). Deposition potential; 3). Etching potential. Results and discussions are shown below.

Deposition time: We investigated the effect of deposition time by altering the number of deposition-etching cycles (See Figure 8a). More cycles correspond to higher deposition time and thicker film formation. As expected, the catalytic activity of the film increased as the number of cycles increased from 2 to 8. The film's thickness reached a plateau above 8 cycles. Thus, 8 cycles were used for the optimized condition.

Deposition potential: -1.7 V was found to be best condition for electrodeposition. At more negative potential (-2.5 V and -2.1 V) we observed extremely vigorous hydrogen

bubbling because of proton reduction. The tremendous amount of H_2 gas generated at the electrode surface certainly inhibited film deposition and growth which can be seen by naked eyes. Since less material was deposited, it led to an inferior HER performance compared to the film deposited at lower applied potential (-1.7 V). At -1.7 V, the deposition process will be more mile and controlled. In contrast, using very low potentials (-1.3 V) produced lower HER activity because of insufficient deposition rate (See Figure 8b)

Etching potential: Etching potential does not have a substantial impact on the film's HER performance (Figure 8c). By changing etching potential, it only changed the rate of etching metallic iron. Given sufficient time, all iron would be etched. The final film has the same chemical structure and components and thus similar HER activity. The potential at -0.1 V vs SCE was used as the final condition.

In addition, we found the electrochemical etching at -0.1 V vs SCE was crucial to remove the excessively co-deposited metallic iron. Without electrochemical etching, the deposited film is unstable under acidic solution. As soon as the un-etched film is exposed to 0.5 M H_2SO_4, there are gas bubbles (H_2) generated at the electrode surface because metallic iron reacts rapidly with sulfuric acid. Thus, etching process was necessary to improve the film's stability. In addition, this method produced phosphide-rich metal based electrocatalysts which were shown to be advantageous for HER and more resilient to corrosion. For instance, previous studies showed that Ni_5P_4 outperforms Ni_2P and $Ni_{12}P_5$ with respect to HER catalysis.[30,31] Moreover, previous studies showed that FeP is more active than Fe_2P towards HER and that FeP_2 nanoarray (η_{-10mA/cm^2} = 61 mV) was a better catalyst than FeP nanoarray(η_{-10mA/cm^2} = 96 mV) in 0.5 M H_2SO_4.[32,33] Hence, the strength of the in-situ etching technique

stems from the ease of selectively stripping less active iron rich areas that interfere with the efficient catalysis by the phosphide rich elements.

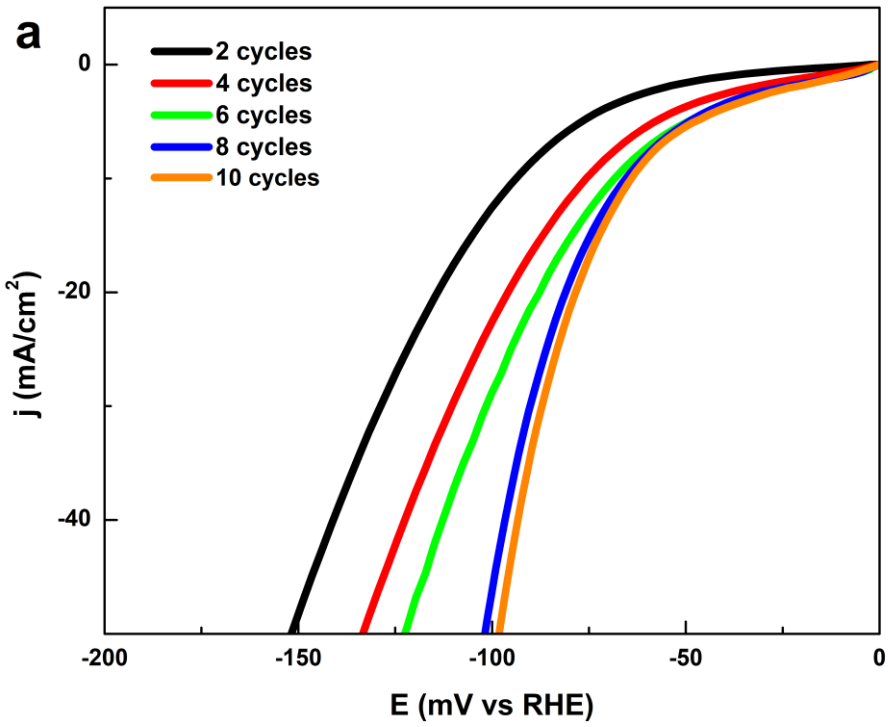

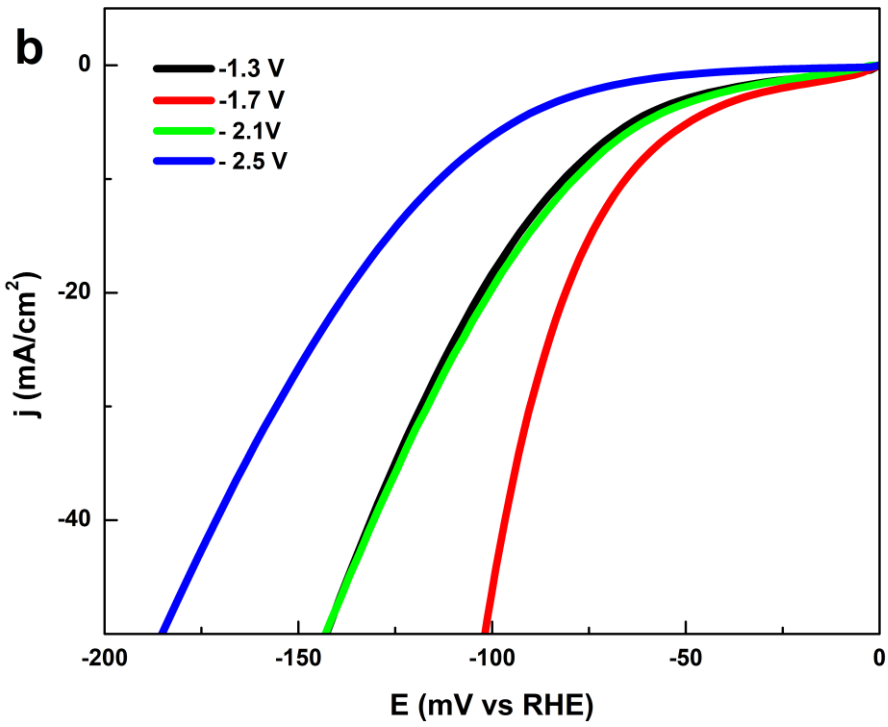

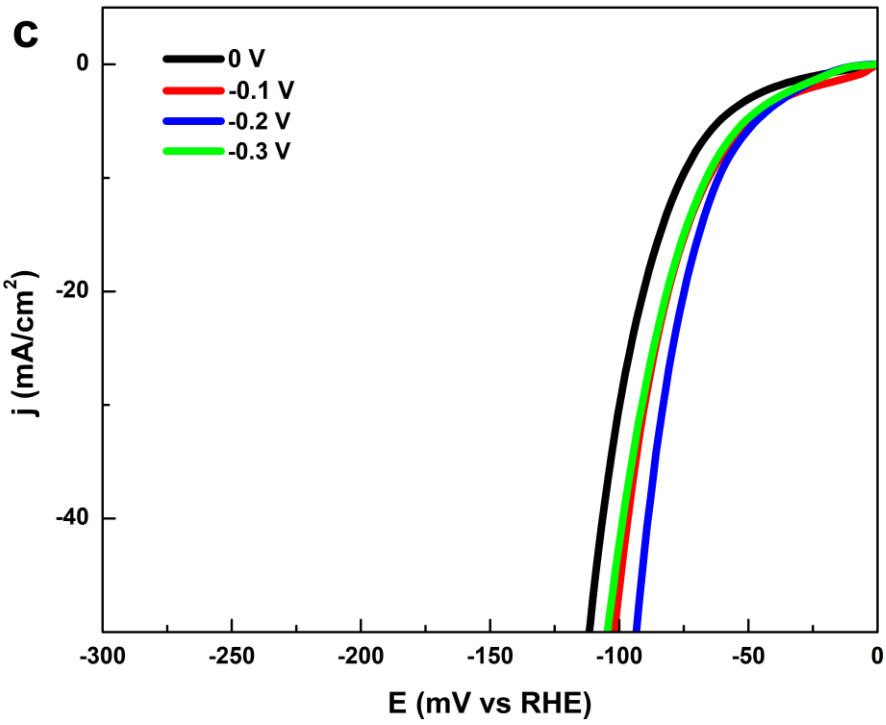

Figure 8. Optimization of the (a) deposition cycles, (b) deposition potential, (c) etching potential. Deposition solution: 0.72 M $FeSO_4 \cdot 7H_2O$, 0.72 M 1.58 g NaH_2PO_2 and 1 vol. % of formic acid in ultrapure water. The pH was adjusted to 1.5 by adding sulfuric acid.

3.3.2. The HER Activity of FeP Film

With the optimized condition in hand, linear sweep voltammetry (LSV) was used to assess the electrocatalytic HER activity of iron phosphide film in acidic (0.5 M H_2SO_4, pH=0.3), neutral (1.0 M phosphate buffer, pH=6.4) and alkaline (1.0 M KOH, pH=14.0) solutions. In each solution, control experiments were first performed to confirm the necessity of each component for the successful deposition of an efficient electrocatalysts. As shown in Figure 9 (a-c, black curve), the copper electrode before electrodeposition had no catalytic ability over the measured potential window. There was no catalytic current if iron precursors (Sample S1,

Figure 9a-c, red curve) or phosphide precursors (Sample S2, Figure 9a-c, green curve) were not added into the deposition solution.

Intriguingly, the addition of formic acid contributed to the formation of a uniform film and enhanced catalytic activity (Sample S3, Figure 9a-c, dark blue curve). In addition, the solution acidity (Sample S4, Figure 9a-c, light blue curve) played a crucial role in the electrodeposition process since low pH facilitated the generation of PH_3 which reduced Fe^{2+} to form a FeP film (Scheme 2).[28,29] The role of formic acid and solution pH were further studied and explained in Section 3.3.3.

In acidic solutions, electrodeposited FeP film only required an overpotential of η= 66 mV (Figure 9, magenta curve) to obtain a current density of -10 mA/cm^2. The result obtained under acidic conditions are unprecedented for the following reasons: I) this is competitively low overpotential even though no complex nanomaterials were needed for preparation (see Section 3.5. Table 3). [23,34–42]As a comparison, the benchmark HER catalyst Pt/C have an overpotential of 29 mV at the current density of -10 mA/cm^2 (Figure 9, orange curve); II) our results did not differ significantly from results obtained using nanostructures prepared by much more complicated methods. (e.g. Callejas et al. reported $\eta_{-10\ mA/cm^2}$ = 50 mV with FeP nanoparticles [18], Chung et al. reported $\eta_{-10\ mA/cm^2}$ = 71 mV with carbon-shell-coated FeP nanoparticles.[20]) Moreover, it was much better than other electrodeposited FeP film ($\eta_{-10\ mA/cm^2}$ =110 mV).[24] Additionally, the FeP film required relatively low over-potentials even at much larger current density (Figure 10) which inferred its applicability on high demanding industrial process.

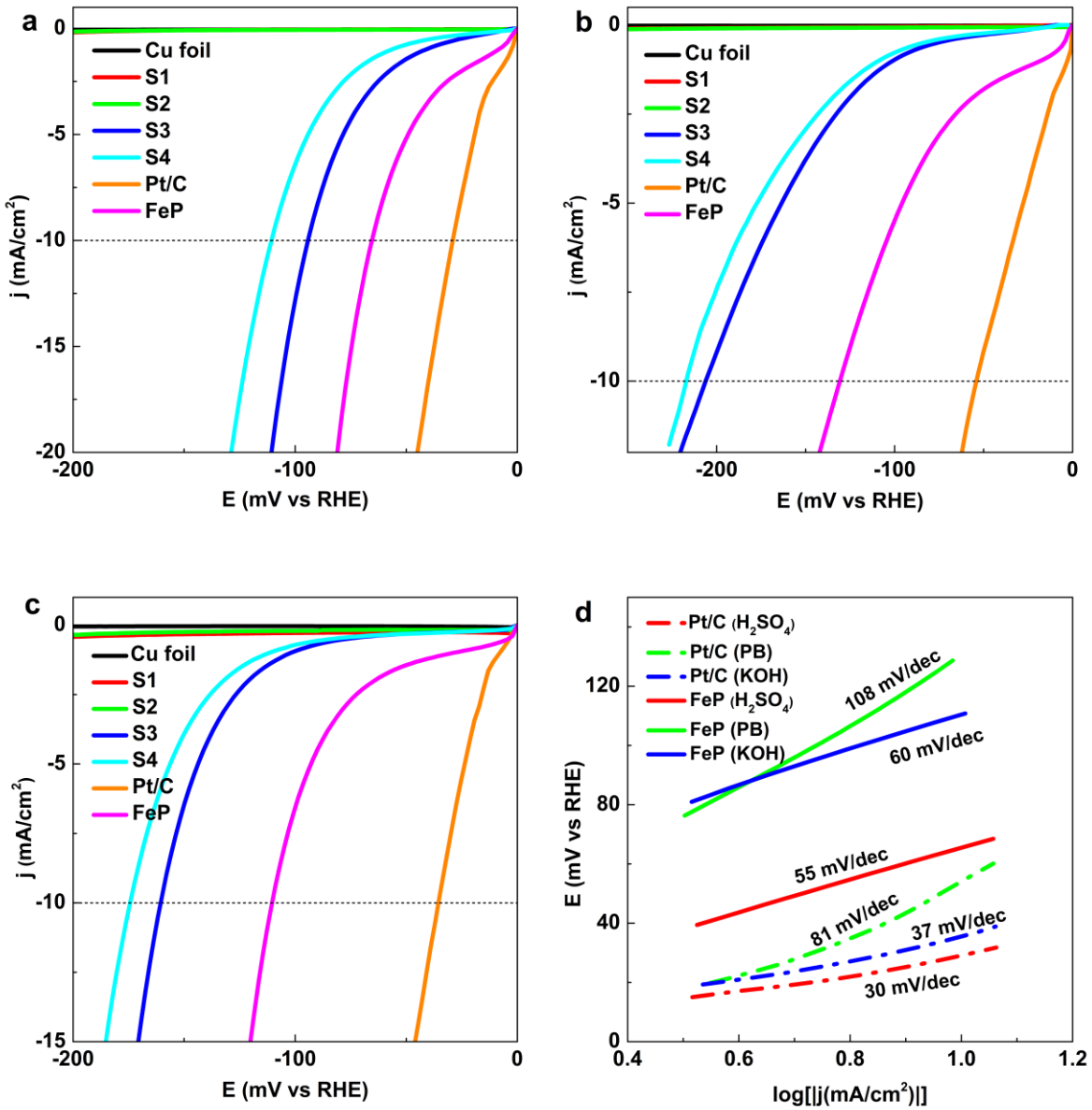

Figure 9. Linear sweep voltammetry recorded at a scan rate of 2 mV/s in (a) 0.5 M H_2SO_4, (b) 1.0 M phosphate buffer, and (c) 1.0 M KOH; Notes: For S1-S4, controls experiments were performed on film obtained without $FeSO_4 \cdot 7H_2O$ (Sample S1), NaH_2PO_2 (Sample S2), HCOOH (Sample S3) and H_2SO_4 (Sample S4) in the deposition solution. (d) Tafel plot of FeP film and Pt/C electrode in acidic, neutral, alkaline solution.

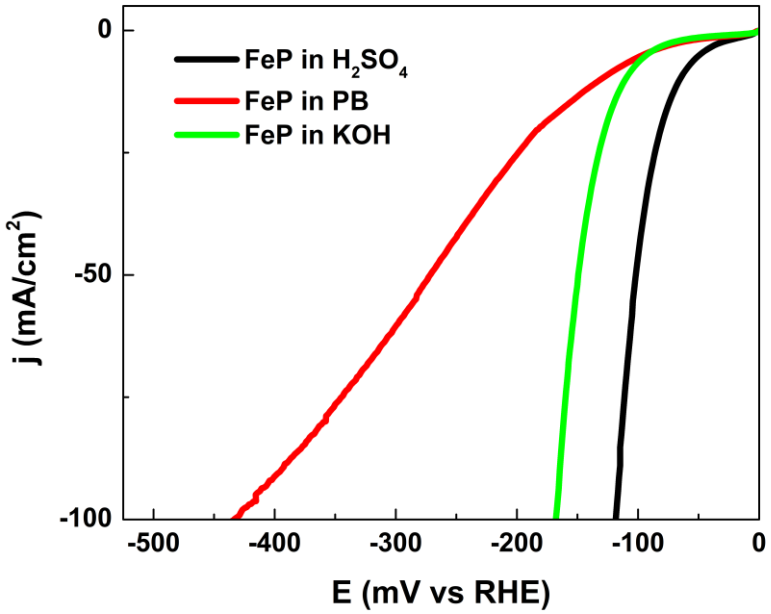

Figure 10. Linear sweep voltammetry of FeP recorded at a scan rate of 2 mV/s in acidic, neutral and alkaline solution in the high current density region.

Next, we investigated the performance of the FeP film electrode in neutral (1.0 M phosphate buffer solution, PB) and alkaline (1.0 M KOH) solutions in order to evaluate the broader applicability of the FeP film over the full pH range. To obtain a current density of -10 mA/cm^2, overpotentials of 131 mV and 110 mV were required under neutral and alkaline conditions, respectively (Figure 9b-c, magenta curve). As for comparison, Pt/C electrode has the overpotentials of 54 mV in neutral solutions and 37 mV in alkaline solutions. In fact, our results are comparable to other electrodeposited materials such as CoS (165 mV at -10 mA/cm^2 in neutral media)[43], CoP (94 mV at -10 mA/cm^2 in alkaline media)[44] and other electrodeposited FeP (140 mV at -10 mA/cm^2 in alkaline media)[24]. For further comparisons among previously reported electrodeposited catalysts under neutral and alkaline conditions, see Section 3.5 Table 3).[24,33,38–50]

We further analyzed the HER kinetics using Tafel plot (log (current density) vs overpotential) in order to evaluate the catalyst performance under various applied overpotentials.[51] In acidic solutions, FeP had a Tafel slope of 55 mV/dec (Figure 9d). In general, Tafel slope represents how much additional overpotentials are required to increase the current density by a decade. Thus, a lower Tafel slope is favored. In our case, the data shows that a low overpotential (55 mV) is additionally needed in order to increase the current density by an order of magnitude under kinetically controlled conditions. These results are comparable with state-of-the-art architecture of related metal phosphides such as Ni_2P/Ti (46 mV/dec),[50] CoP/Ti (50 mV/dec),[45] and FeP/C (52 mV/dec)[20], and it is very similar to other electrodeposited FeP (59 mv/dec)[24]. Moreover, the exchange current density was 6.3×10^{-4} A/cm^2 based on Tafel plot. This is slightly better than FeP nanoparticle (4.3×10^{-4} A/cm^2)[18] and FeP nanoarray (4.2×10^{-4} A/cm^2)[21]. Moreover, the FeP electrode had Tafel slopes of 108 mV/dec in neutral solutions and 60 mV/dec in alkaline solutions, which are comparable to other leading metal phosphide materials. (See Section 3.5. Table 3)

To further understand HER kinetics, electrochemical impedance spectra (EIS) were performed and the data was fitted using an equivalent circuit. (See Figure 11). Charge transfer resistance (R_{ct}) of Pt/C, FeP, sample S3 and sample S4 electrode were compared in acidic, neutral and alkaline solutions. As listed in Table 1, the R_{ct} value of FeP electrode was only 4.6 Ω in acidic solution. In general, R_{ct} decreases in an order of Pt/C<FeP<sample S3<sample S4. Lower Rct corresponds to higher HER activity. Therefore, the EIS spectra were in well agreement with voltammetric studies where Pt/C>FeP>sample S3>sample S4 in terms of HER activity. Overall, it revealed the fast kinetics of electrodeposited FeP towards HER under all-pH conditions.

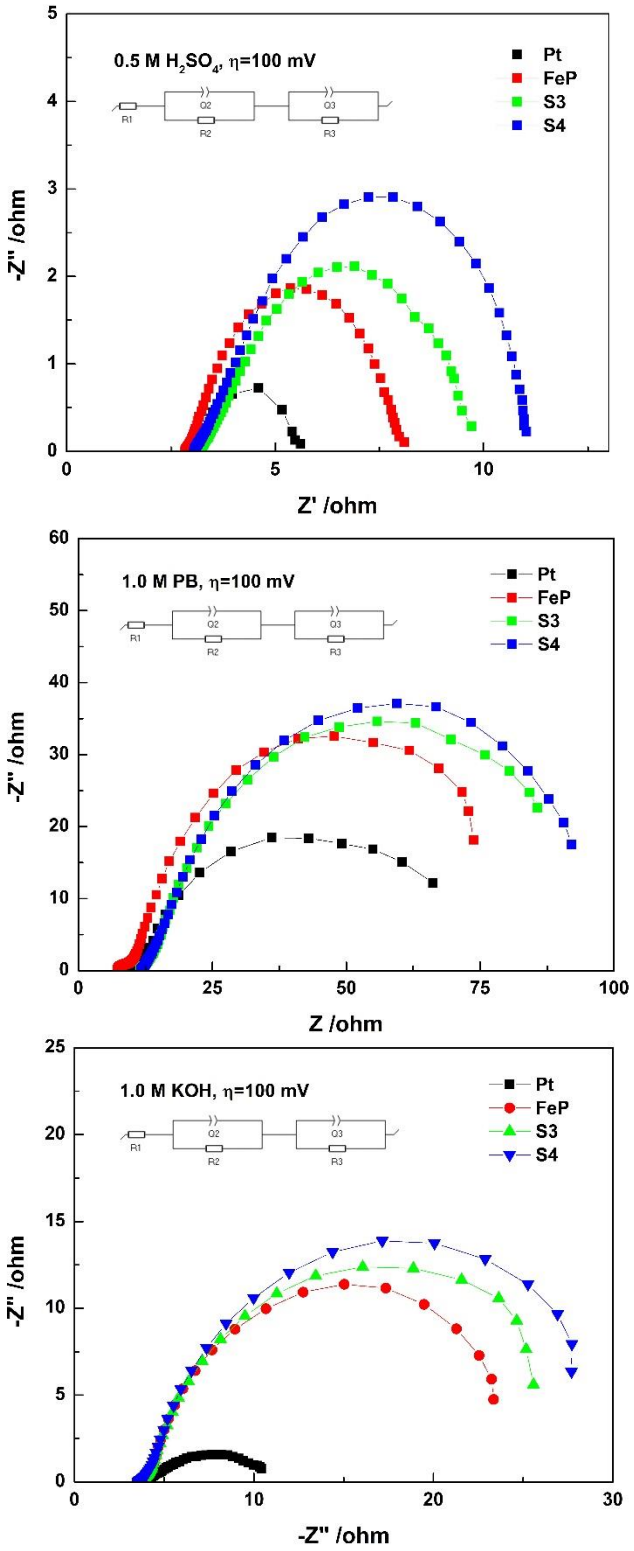

Figure 11. EIS spectra of Pt/C, FeP, sample S3 and sample S4 electrode. Note: Sample S3: film deposited without formic acid in deposition solution; Sample S4: film deposited without

sulfuric acid in deposition solution; Equivalent circuits: R1: solution resistance; Q2: constant phase element of the film; R2: resistance of the film, Q3: constant phase element of double layer, R3: charge transfer resistance R_{ct}.

Electrode	R_{ct} in 0.5 M H_2SO_4 (Ω)	R_{ct} in 1.0 M PB (Ω)	R_{ct} in 1.0 M KOH (Ω)
Pt	2.2	58.8	5.3
FeP	4.6	75.8	23.1
S3	5.6	82.4	27.3
S4	6.4	83.2	30.6

Table 1. Charge transfer resistance R_{ct} of Pt/C, FeP, sample S3 and sample S4 electrode.

At last, faradaic efficiency (FE) was measured based on the relationship between hydrogen amounts generated and charges consumed. As shown in Figure 12, nearly 100 % FE were obtained in either acidic, neutral, or alkaline solutions. Thus, nearly all charges had been selectively used to reduce proton and generate hydrogen.

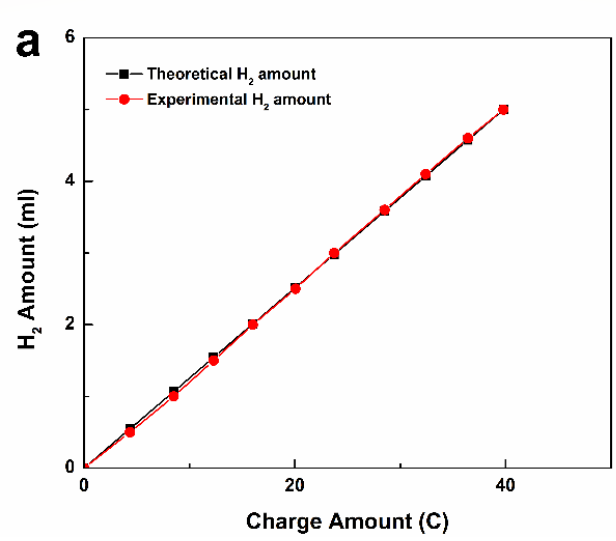

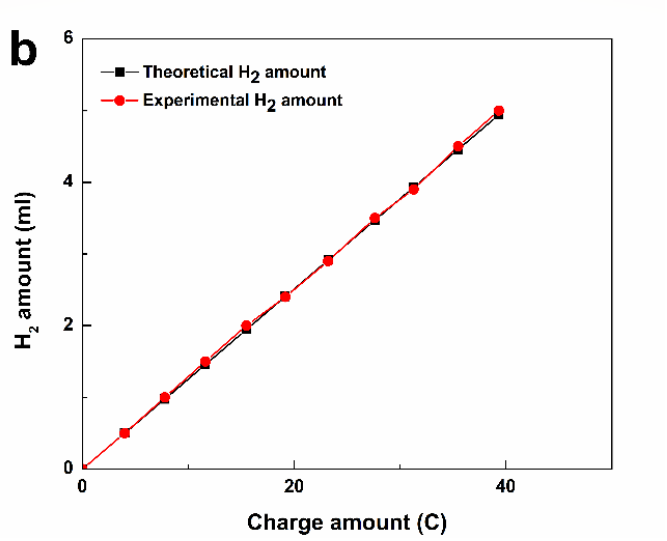

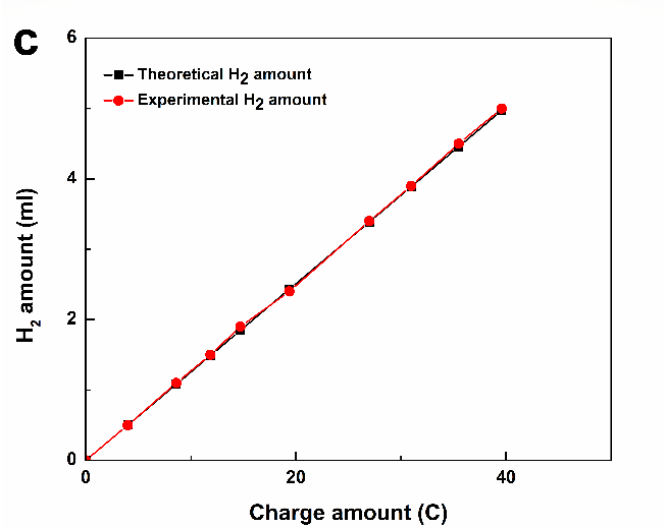

Calculation of faradaic efficiency

$$n(theo, H_2) = \frac{I * t}{2 * \left(96485 \frac{C}{mol}\right)}, \qquad \text{I} = 0.010 \text{ A}$$

$$then, \qquad V(theo, H_2) = \frac{nRT}{P}, \qquad \text{T} = 298.15 \text{ K}, \qquad \text{P} = 101.591 \text{ kPa}$$

$$\boldsymbol{Faradaic\ efficiency} = \frac{V(exp, H_2)}{V(theo, H_2)}$$

Figure 12. Faradic efficiency of FeP in (a) 0.5 M H_2SO_4, (b) 1.0 M PB, (c) 1.0 M KOH.

3.3.3. The Role of Formic Acid and Solution pH

As mentioned previously in section 3.3.2., the formic acid and solution pH were of great importance to FeP film's HER activity (Figure 9, sample S3 & S4). To further understand the role of formic acid and solution acidity during the electrodeposition, four methods were used: I) cyclic voltammetry; II) capacitance and electrochemically active surface area (ECSA) studies; III) electron microscopy; IV) ICP-MS. The results of cyclic voltammetry are shown in Figure 13. The reduction of $FeSO_4$ began at -1.00 V vs SCE. The addition of NaH_2PO_2 only slightly changed the onset potential into -0.91 V vs SCE which indicates a high energy barrier for FeP deposition. However, the onset potential was significantly reduced to -0.68 V vs SCE by adding formic acid and adjusting pH into 1.5. It can be explained that the higher proton concentration facilitates the reduction of hypophosphite ion (Scheme 2, equation 1) as well as FeP deposition. Besides, formic acid may stabilize charged intermediates and thus decrease the energy barrier for electrodeposition.

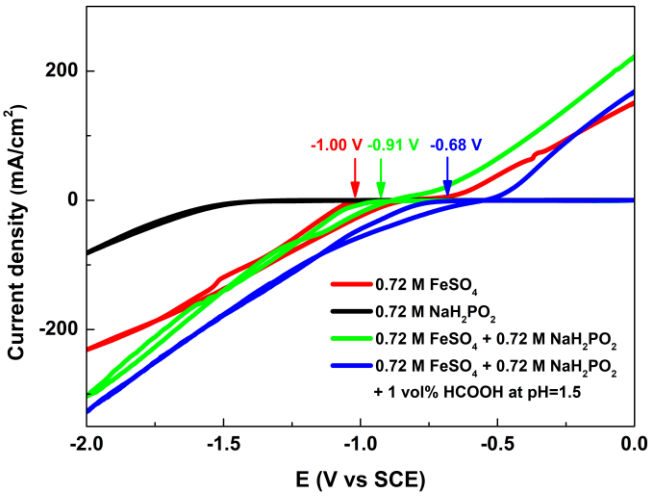

Figure 13. Cyclic voltammetry of Cu electrodes at the scan rate of 100 mV/s in the solutions of 0.72 M $FeSO_4$, 0.72 M NaH_2PO_2, 0.72 M $FeSO_4$+0.72 M NaH_2PO_2, 0.72 M $FeSO_4$+0.72 M NaH_2PO_2+1 vol% HCOOH at pH=1.5, respectively.

In addition to mechanistic benefits, the electrochemical active surface area was compared for FeP film deposited at various condition. The double layer charging region was used to determine the capacitance and to extract the electrochemical active surface area (Figure 14). FeP film deposited at the optimized condition had a capacitance of 444 mF/cm^2, while it substantially dropped into 154 mF/cm^2 or 217 mF/cm^2 without the addition of formic acid or pH adjustment, respectively. It clearly demonstrated that formic acid and solution acidity somehow contributed to a larger surface area of film.

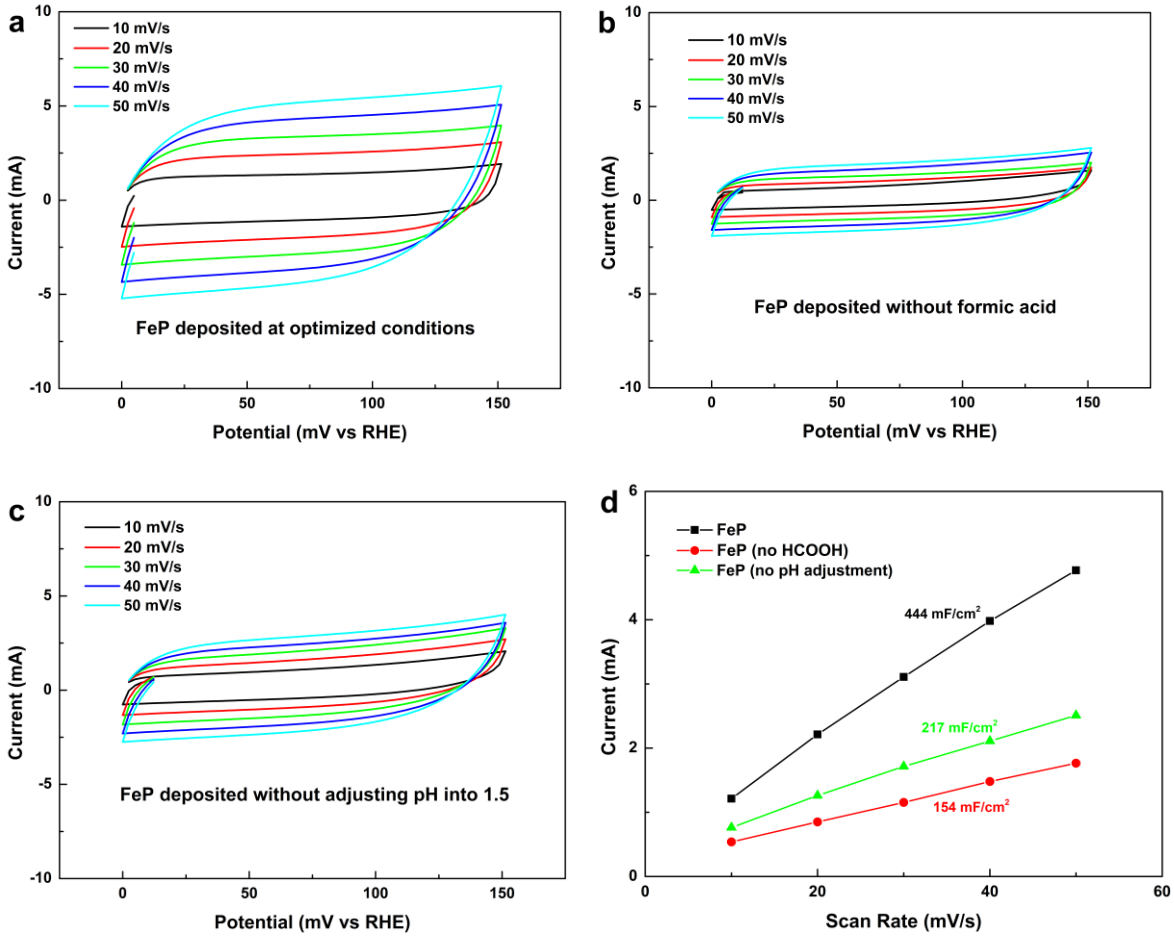

Figure 14. Cyclic voltammograms recorded for FeP film deposited at (a) optimized conditions, (b) no formic acid additives, (c) no pH adjustment into 1.5, in 0.5 M H_2SO_4 at various scan rates in the double layer charging region. (d) Plot of capacitive current obtained at 75 mV vs

RHE against scan rate, and capacitive current= (|forward scan current| + |reverse scan current|)/2.

Intrigued by the surface area change, electron microscopy was used to observe morphological changes. SEM images of various FeP films were collected (Figure 15). The uniformed FeP film is only formed under the optimized conditions. Both formic acid and sulfuric acid are crucial for a sufficient film growth and high film coverage. This explained the ECSA difference observed previously. To understand how the chemical structure of FeP film is changed by formic acid and solution acidity, we used ICP-MS to determine the Fe to P ratio of films. As listed on Table 2, the Fe to P ratio was 1.03 when FeP film was deposited under optimized conditions. This ratio was slightly higher (Fe:P=1.09) if formic acid was omitted from solution. However, it significantly increased to 1.90 if the film was deposited from a solution without addition of sulfuric acid. Again, it seems that low pH and high proton concentration facilitate the deposition of element P which corroborates the mechanism shown on Scheme 2 equation 1. The relatively higher Fe to P ratio may also relate to the lower HER activity of the corresponding film.

(a). 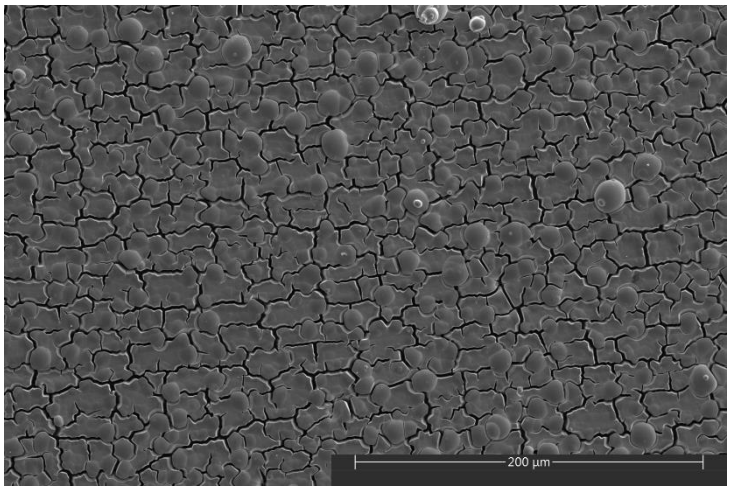

(b). 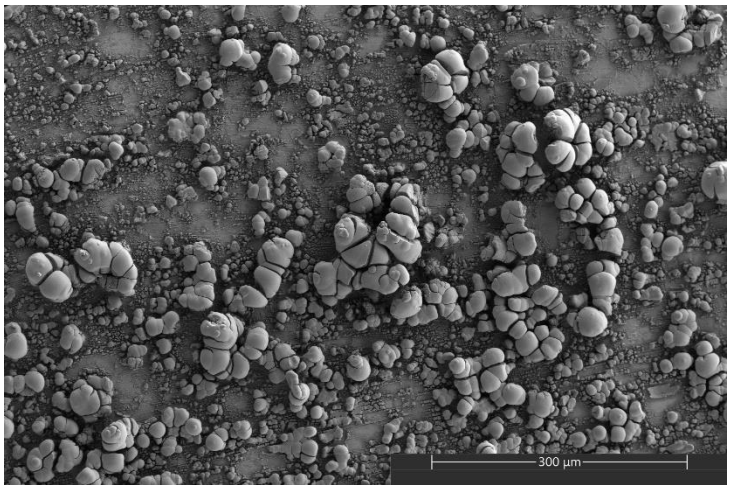

(c). 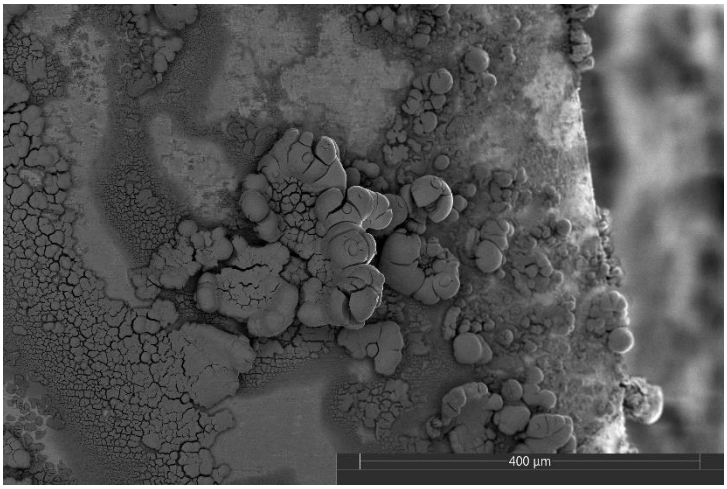

Figure 15. SEM images of FeP film deposited from (a) optimized deposition solution, (b) deposition solution without formic acid added, (c) deposition solution without sulfuric acid added.

Sample	Fe to P ratio
FeP (optimized solution)	1.03
FeP (solution w/o formic acid, pH=1.5)	1.09
FeP (solution w/o sulfuric acid, pH=2.2)	1.90

Table 2. Fe to P ratio analysis (from ICP-MS) of the films deposited from different solutions; Optimized solution: 0.72 M $FeSO_4 \cdot 7H_2O$, 0.72 M NaH_2PO_2 and 1 vol. % formic acid in ultrapure water. The pH was adjusted to 1.5 by adding sulfuric acid.

3.4. Stability

To test FeP film stability, the HER was examined under continuous operation using a constant current density of -10 mA/cm^2. As shown in Figure 16, the FeP was exceptionally stable in acidic and neutral solutions, while relatively less stable in alkaline solutions. In acidic solutions, the overpotentials increased diminutively 7 mV after 24 hours of electrocatalysis (Figure 16, black curve). Similarly, only a 10 mV increase in overpotential was observed in neutral solution (Figure 16, red curve). For comparison, the overpotential of FeP nanoparticle modified electrode increased by 52 mV in acidic solution and 35 mV in neutral solution, over a shorter time period of 16 hours.[18] Under basic conditions, a significant change (51 mV over 24 hours) in overpotential was observed (Figure 16, green curve). In this case, it is worth noting that the overpotential only increased significantly in the first few hours then changed very slowly thereafter. We believe this feature supports that FeP film could be a stable catalyst for long term service, even though there is an initial slight loss of activity under alkaline conditions.

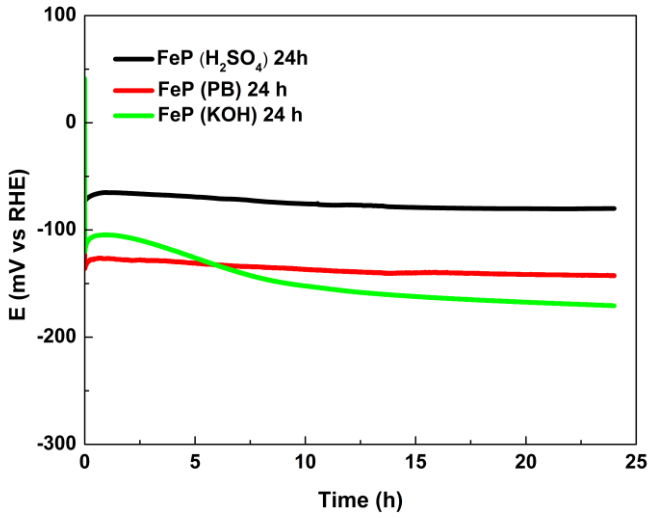

Figure 16. Potential-time response of the HER conducted in acidic, neutral, or alkaline solutions at -10 mA/cm^2 over 24 hours.

Intrigued by the dependence of the film stability on the media pH, we further characterized the FeP film via microscopy and spectroscopy to observe the corresponding changes after HER reaction. It is worth noting that the morphology of the FeP electrode did not change even after 10 hours of electrolysis in acidic, neutral or alkaline solutions at a current density of -10 mA/cm^2, which reconfirmed the high corrosion resistance of FeP electrode (Figure 17). To illustrate the elemental changes after HER, the EDX of FeP films after 10 hours of electrolysis were collected. Compared to the as-deposited film prior to catalysis, peaks of copper became notably higher which indicated the exposure of copper foil substrate and the thinning of FeP film (Figure 18). For the as-deposited FeP film, the ratio of Fe to P was 1.62. After 10 hours of electrolysis in acidic and neutral solution, the Fe:P ratio slightly changed to 1.39 and 1.61, respectively, suggesting that the film integrity was not compromised during long continuous catalysis. However, the phosphide content tremendously decreased after catalyzing HER in alkaline solutions, eventually reaching a Fe:P ratio of 3.16. The EDX results coincided with

the stability test results shown in Figure 16 and all together reflected a stable, morphologically resilient structure under acidic and neutral solutions. The slight instability in alkaline solution can be attributed to possible dissolution of phosphorous.

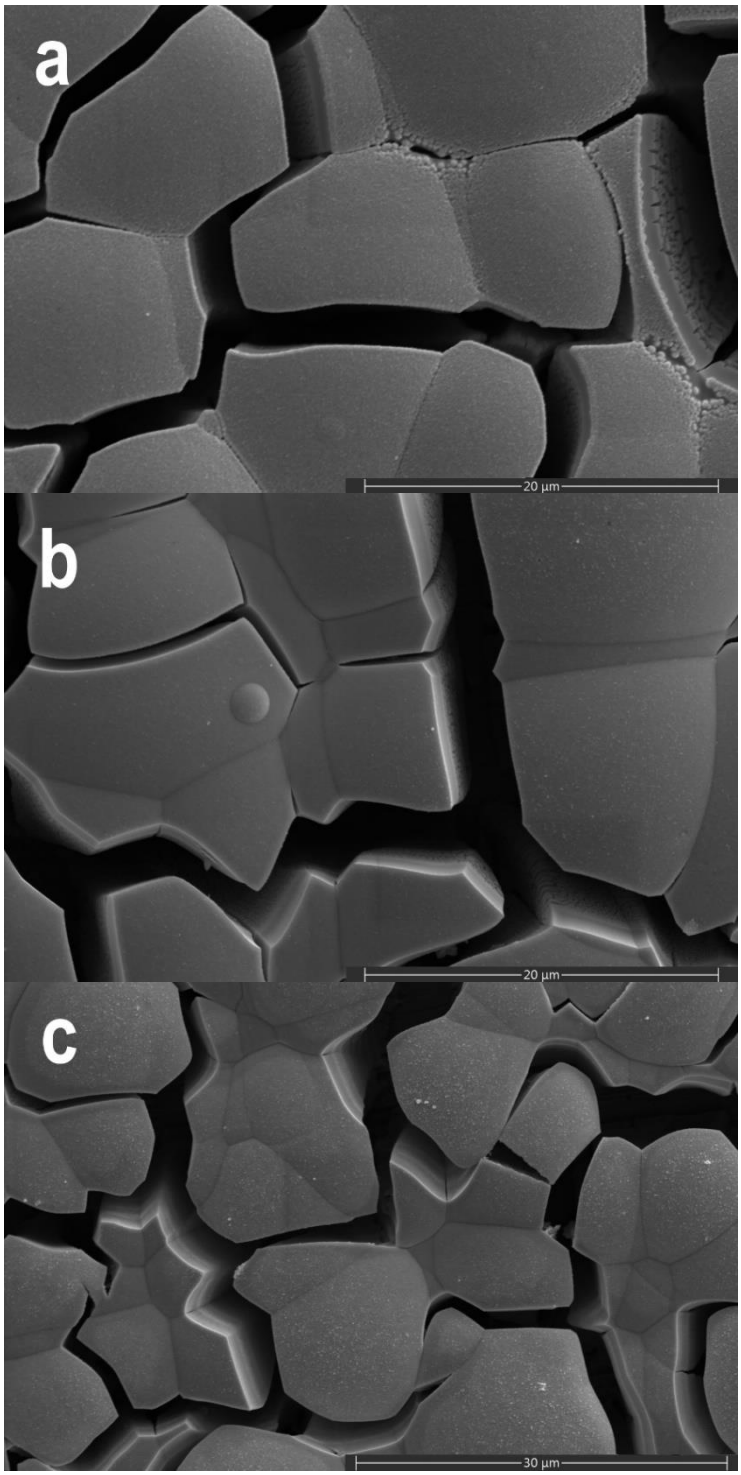

Figure 17. SEM images of FeP films after 10 h of HER at a current density of -10 mA/cm^2 in (a) 0.5 M H_2SO_4, (b) 1.0 M PB, (c) 1.0 M KOH.

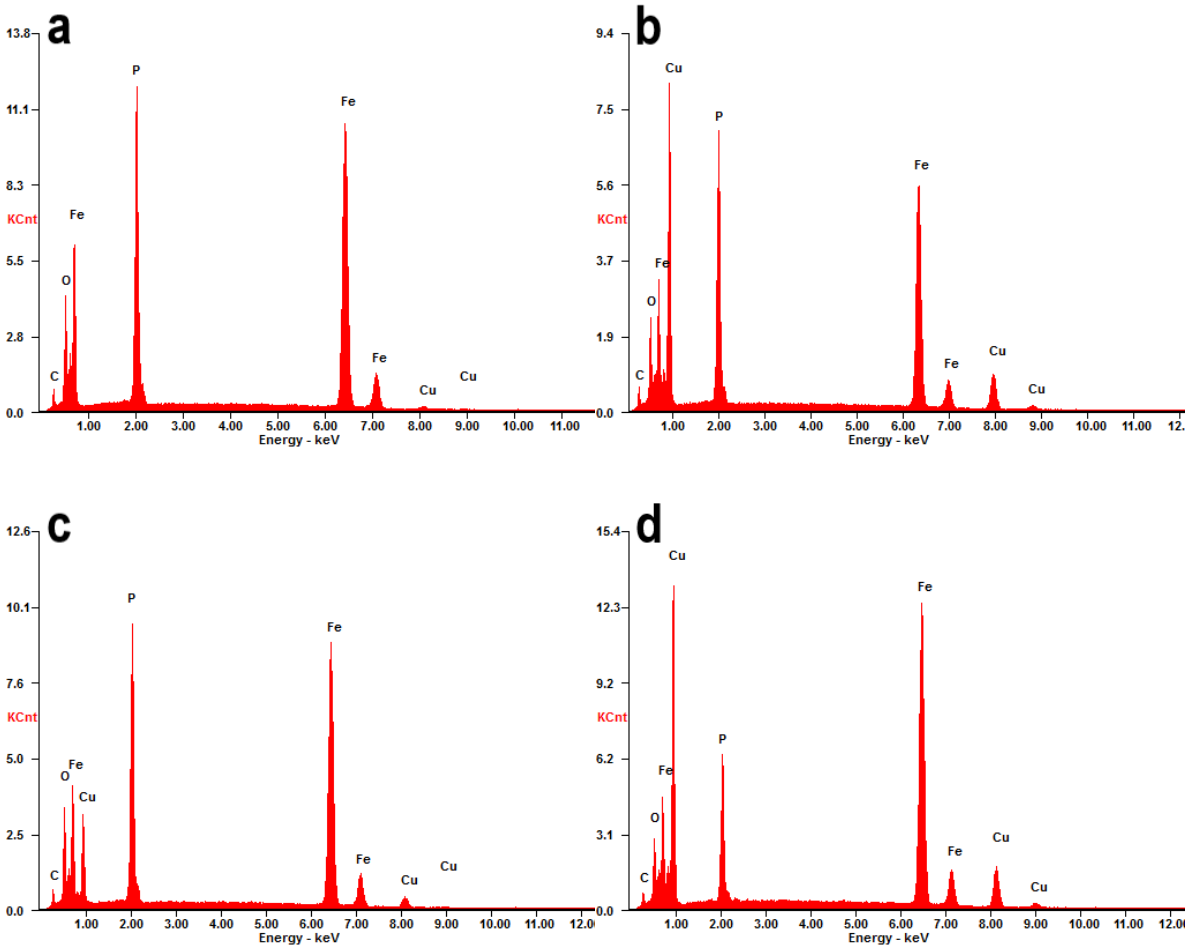

Figure 18. EDX of FeP films (a) as-deposited, (b) after 10 h of HER in 0.5 M H_2SO_4, (c) after 10 h of HER in 1.0 M PB, (d) after 10 h of HER in 1.0 M KOH.

X-ray photoelectron spectroscopy (XPS) analysis was performed on the as-deposited and post-HER electrodes to study compositions change on FeP film. As shown in Figure 19, peaks corresponding to oxidized iron species (710.5 eV, 724.0 eV) and phosphate (132.9 eV) were much higher after HER. On the other hand, the peaks of Fe^{3+} in FeP (707.1 eV, 720.1 eV)

virtually disappeared in alkaline conditions. Consequently, the XPS results are in-line with our stability and EDX measurements and indicates that FeP might be converted into iron oxides or iron oxide-hydroxide during catalysis in alkaline solutions as similar phenomenon has been observed on Co_2P.[52]

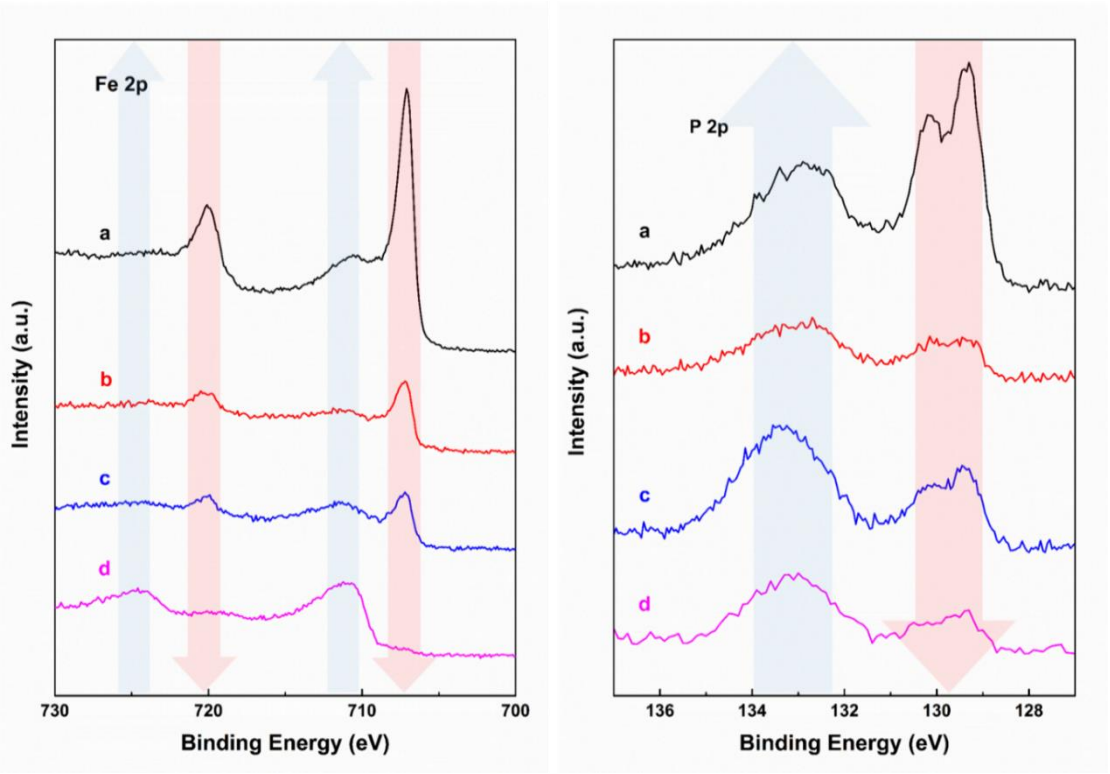

Figure 19. XPS spectra of Fe 2p and P 2p in various FeP films; (a) as-deposited; (b) after 10 h of HER in 0.5 M H_2SO_4; (c) after 10 h of HER in 1.0 M PB; (d) after 10 h of HER in 1.0 M KOH.

3.5. Comparison with Other Electrocatalysts

The comparison of electrodeposited FeP with other selected electrocatalysts were shown in Table 3. The overpotential at -10 mA/cm^2 was used to assess catalyst's HER activity. The Tafel slope was used to compare catalyst's HER kinetics.

Electrode material	Electrolyte	η (-10 mA/m^2)	Tafel slope (mV/dec)	Reference
CoP	0.5 M H_2SO_4	85	50	[34]
Mo-P-S	0.5 M H_2SO_4	200	36	[35]
Co-doped $NiSe_2$	0.5 M H_2SO_4	212	42	[36]
CoSe	0.5 M H_2SO_4	135	62	[37]
polymorphic $CoSe_2$	0.5 M H_2SO_4	70	31	[38]
$Ni/Ni(OH)_2$	0.5 M H_2SO_4	190 (20 mA/cm^2)	116	[39]
Ni-Cu-P	0.5 M H_2SO_4	150	69	[40]
Cu-Co-P	0.5 M H_2SO_4	262	59	[53]
FeP	0.5 M H_2SO_4	110	59	[24]
FeP	**0.5 M H_2SO_4**	**66**	**55**	**this work**
CoS	1.0 M PB	165	93	[43]
Ni-Co-S	1.0 M PB	280	93	[54]
NiP_x	1.0 M PB	230	101	[55]
$CoW(OH)_x$	1.0 M PB	74	150	[56]
FeP	**1.0 M PB**	**131**	**108**	**this work**
$Fe_{87}P_{13}$	1.0 M KOH	375	115	[23]
CoP	1.0 M KOH	94	42	[44]
Mo-S-P	1.0 M KOH	350	104	[35]
Co-Fe-P	1.0 M KOH	169	57	[57]
Co-doped $NiSe_2$	1.0 M KOH	64	63	[36]
$NiSe_2$	1.0 M KOH	96	82	[46]
Co-Ni-P	1.0 M KOH	103	33	[47]
Ni-Co-P	1.0 M KOH	30	41	[48]
Ni-Cu-P	1.0 M KOH	120	69	[40]
Co-Fe-P	1.0 M KOH	73	43	[49]
NiP_x	1.0 M KOH	105	45	[58]
Cu–Co–P	1.0 M KOH	231	86	[53]
Ni-S	1.0 M KOH	330	77	[59]
Co/CoP	1.0 M KOH	35	71	[60]
Ni-P	1.0 M KOH	93	43	[61]
FeP	1.0 M KOH	140	62	[24]
FeP	**1.0 M KOH**	**110**	**60**	**this work**

Table 3. Comparison of electrodeposited FeP with other HER catalysts.

Chapter 4. Conclusions

We have developed a straightforward electrodeposition process to synthesize FeP film from earth-abundant iron and phosphorus precursors at room temperature. This method is much simpler and greener compared to conventional synthesis by high-temperature solution-phase reaction or gas-solid phosphorization reaction. The deposition process includes electrodeposition at -1.7 V vs SCE followed by in-situ selective etching of metallic iron under an applied potential of -0.1 V. The in-situ etching is crucial to improve the catalyst's stability. Formic acid and low solution pH can mechanistically facilitate the film deposition as evidenced by cyclic voltammetry. In addition, the film's surface area was increased as shown in capacitance studies and electron microscopy studies. Moreover, ICP-MS studies demonstrated that low solution pH was of great importance to phosphide deposition which correlated well with the purposed deposition mechanism.

The as-deposited film was fully characterized by SEM, TEM, EDX, XPS, and ICP-MS, and it was confirmed to be amorphous iron phosphide with a very high electrochemically active surface area. This catalyst exhibits excellent HER activity over the full pH range and functions favorably when compared to other precious metals based or delicately synthesized catalysts. Its HER kinetics were fast according to Tafel slope analysis and EIS studies. A Small Tafel slope and very low charge transfer resistance were observed under acidic conditions. Finally, this material retains remarkable stability over long-term continuous reaction in acidic and neutral solutions, making it a practical electrocatalyst for industrial applications. The good stability was explained by the negligible morphological changes and chemical structure changes after long term HER reaction. In contrast, the relative instability of FeP film under basic HER condition was believed to be the dissolution of element

phosphorus and the conversion of iron phosphide into iron oxide or iron oxide-hydroxide as evidenced by XPS and EDX. The main conclusion of this work is that a carefully controlled electrochemical deposition can outcompete complex materials synthesis for certain applications. Although it is typically attractive to think about and design fancy 3-D structures that exhibit interesting catalytic activities, sometimes the incremental idealization of a much simpler process is a better synthetic route. Proper electrochemical control of cost-effective catalysts such as FeP that outcompetes most of the known complex earth-abundant catalyst is such an example that was discovered here.

Reference:

(1) Dincer, I. Renewable Energy and Sustainable Development: A Crucial Review. *Renew. Sustain. Energy Rev.* **2000**, *4*, 157–175.

(2) Hussain, A.; Arif, S. M.; Aslam, M. Emerging Renewable and Sustainable Energy Technologies: State of the Art. *Renew. Sustain. Energy Rev.* **2017**, *71*, 12–28.

(3) Mazloomi, K.; Gomes, C. Hydrogen as an Energy Carrier: Prospects and Challenges. *Renew. Sustain. Energy Rev.* **2012**, *16*, 3024–3033.

(4) Ahluwalia, R. K.; Peng, J. K. Automotive Hydrogen Storage System Using Cryo-Adsorption on Activated Carbon. *Int. J. Hydrogen Energy* **2009**, *34*, 5476–5487.

(5) Abe, J. O.; Popoola, A. P. I.; Ajenifuja, E.; Popoola, O. M. Hydrogen Energy, Economy and Storage: Review and Recommendation. *Int. J. Hydrogen Energy* **2019**, *44*, 15072–15086.

(6) Van Hook, J. P. Methane-Steam Reforming. *Catal. Rev.* **1980**, *21*, 1–51.

(7) Eftekhari, A. Electrocatalysts for Hydrogen Evolution Reaction. *Int. J. Hydrogen Energy* **2017**, *42*, 11053–11077.

(8) Jiao, Y.; Zheng, Y.; Jaroniec, M.; Qiao, S. Z. Design of Electrocatalysts for Oxygen- and Hydrogen-Involving Energy Conversion Reactions. *Chem. Soc. Rev.* **2015**, *44*, 2060–2086.

(9) McCrory, C. C. L.; Jung, S.; Ferrer, I. M.; Chatman, S. M.; Peters, J. C.; Jaramillo, T. F. Benchmarking Hydrogen Evolving Reaction and Oxygen Evolving Reaction Electrocatalysts for Solar Water Splitting Devices. *J. Am. Chem. Soc.* **2015**, *137*, 4347–4357.

(10) Zeng, M.; Li, Y. Recent Advances in Heterogeneous Electrocatalysts for the Hydrogen Evolution Reaction. *J. Mater. Chem. A.* **2015**, *3*, 14942–14962.

(11) Vesborg, P. C. K.; Seger, B.; Chorkendorff, I. Recent Development in Hydrogen Evolution Reaction Catalysts and Their Practical Implementation. *J. Phys. Chem. Lett.* **2015**, *6*, 951–957.

(12) Xiao, P.; Chen, W.; Wang, X. A Review of Phosphide-Based Materials for Electrocatalytic Hydrogen Evolution. *Adv. Energy Mater.* **2015**, *5*, 1500985.

(13) Shi, Y.; Zhang, B. Recent Advances in Transition Metal Phosphide Nanomaterials: Synthesis and Applications in Hydrogen Evolution Reaction. *Chem. Soc. Rev.* **2016**, *45*, 1529–1541.

(14) Callejas, J. F.; Read, C. G.; Roske, C. W.; Lewis, N. S.; Schaak, R. E. Synthesis, Characterization, and Properties of Metal Phosphide Catalysts for the Hydrogen-Evolution Reaction. *Chem. Mater.* **2016**, *28*, 6017–6044.

(15) Gao, M.-R.; Xu, Y.-F.; Jiang, J.; Yu, S.-H. Nanostructured Metal Chalcogenides: Synthesis, Modification, and Applications in Energy Conversion and Storage Devices. *Chem. Soc. Rev.* **2013**, *42*, 2986.

(16) Anantharaj, S.; Ede, S. R.; Sakthikumar, K.; Karthick, K.; Mishra, S.; Kundu, S. Recent Trends and Perspectives in Electrochemical Water Splitting with an Emphasis on Sulfide, Selenide, and Phosphide Catalysts of Fe, Co, and Ni: A Review. *ACS Catal.* **2016**, *6*, 8069–8097.

(17) Michalsky, R.; Zhang, Y. J.; Peterson, A. A. Trends in the Hydrogen Evolution Activity of Metal Carbide Catalysts. *ACS Catal.* **2014**, *4*, 1274–1278.

(18) Callejas, J. F.; McEnaney, J. M.; Read, C. G.; Crompton, J. C.; Biacchi, A. J.; Popczun, E. J.; Gordon, T. R.; Lewis, N. S.; Schaak, R. E. Electrocatalytic and Photocatalytic Hydrogen Production from Acidic and Neutral-PH Aqueous Solutions Using Iron Phosphide Nanoparticles. *ACS Nano* **2014**, *8*, 11101–11107.

(19) Qian, C.; Kim, F.; Ma, L.; Tsui, F.; Yang, P.; Liu, J. Solution-Phase Synthesis of Single-Crystalline Iron Phosphide Nanorods/Nanowires. *J. Am. Chem. Soc.* **2004**, *126*, 1195–1198.

(20) Chung, D. Y.; Jun, S. W.; Yoon, G.; Kim, H.; Yoo, J. M.; Lee, K. S.; Kim, T.; Shin, H.; Sinha, A. K.; Kwon, S. G.; et al. Large-Scale Synthesis of Carbon-Shell-Coated FeP Nanoparticles for Robust Hydrogen Evolution Reaction Electrocatalyst. *J. Am. Chem. Soc.* **2017**, *139*, 6669–6674.

(21) Jiang, P.; Liu, Q.; Liang, Y.; Tian, J.; Asiri, A. M.; Sun, X. A Cost-Effective 3D Hydrogen Evolution Cathode with High Catalytic Activity: FeP Nanowire Array as the Active Phase. *Angew. Chem. Int. Ed.* **2014**, *53*, 12855–12859.

(22) Tian, L.; Yan, X.; Chen, X. Electrochemical Activity of Iron Phosphide Nanoparticles in Hydrogen Evolution Reaction. *ACS Catal.* **2016**, *6*, 5441–5448.

(23) Sequeira, C. A. C. A. C.; Santos, D. M. F. M. F.; Brito, P. S. D. S. D. Electrocatalytic Activity of Simple and Modified Fe–P Electrodeposits for Hydrogen Evolution from Alkaline Media. *Energy* **2011**, *36*, 847–853.

(24) Shi, J.; Qiu, F.; Yuan, W.; Guo, M.; Yuan, C.; Lu, Z. H. Novel Electrocatalyst of Nanoporous FeP Cubes Prepared by Fast Electrodeposition Coupling with Acid-Etching for Efficient Hydrogen Evolution. *Electrochim. Acta* **2020**, *329*, 135185.

(25) Carmo, M.; Fritz, D. L.; Mergel, J.; Stolten, D. A Comprehensive Review on PEM Water Electrolysis. *Int. J. Hydrogen Energy* **2013**, *38*, 4901–4934.

(26) Kundu, A.; Sahu, J. N.; Redzwan, G.; Hashim, M. A. An Overview of Cathode Material and Catalysts Suitable for Generating Hydrogen in Microbial Electrolysis Cell. *Int. J. Hydrogen Energy* **2013**, *38*, 1745–1757.

(27) LEROY, R. Industrial Water Electrolysis: Present and Future. *Int. J. Hydrogen Energy* **1983**, *8*, 401–417.

(28) Chun, Y.-M.; Shin, H.-C. Electrochemical Synthesis of Iron Phosphides as Anode Materials for Lithium Secondary Batteries. *Electrochim. Acta* **2016**, *209*, 369–378.

(29) Park, I. T.; Shin, H. C. Amorphous FePy($0.1 < y < 0.7$) Thin Film Anode for Rechargeable Lithium Battery. *Electrochem. commun.* **2013**, *33*, 102–106.

(30) Kucernak, A. R. J.; Naranammalpuram Sundaram, V. N. Nickel Phosphide: The Effect of Phosphorus Content on Hydrogen Evolution Activity and Corrosion Resistance in Acidic Medium. *J. Mater. Chem. A* **2014**, *2*, 17435–17445.

(31) Pan, Y.; Liu, Y. Y. Y.; Zhao, J.; Yang, K.; Liang, J.; Liu, D. D. D.; Hu, W.; Liu, D. D. D.; Liu, Y. Y. Y.; Liu, C. Monodispersed Nickel Phosphide Nanocrystals with Different Phases: Synthesis, Characterization and Electrocatalytic Properties for Hydrogen Evolution. *J. Mater. Chem. A* **2015**, *3*, 1656–1665.

(32) Cho, G.; Kim, H.; Park, Y. S.; Hong, Y. K.; Ha, D. H. Phase Transformation of Iron Phosphide Nanoparticles for Hydrogen Evolution Reaction Electrocatalysis. *Int. J. Hydrogen Energy* **2018**, *43*, 11326–11334.

(33) Son, C. Y.; Kwak, I. H.; Lim, Y. R.; Park, J. FeP and FeP2 Nanowires for Efficient Electrocatalytic Hydrogen Evolution Reaction. *Chem. Commun.* **2016**, *52*, 2819–2822.

(34) Saadi, F. H.; Carim, A. I.; Verlage, E.; Hemminger, J. C.; Lewis, N. S.; Soriaga, M. P. CoP as an Acid-Stable Active Electrocatalyst for the Hydrogen-Evolution Reaction: Electrochemical Synthesis, Interfacial Characterization and Performance Evaluation. *J. Phys. Chem. C* **2014**, *118*, 29294–29300.

(35) Sultana, U. K.; O'Mullane, A. P. Electrochemical Formation of Amorphous Molybdenum Phosphosulfide for Enabling the Hydrogen Evolution Reaction in Alkaline and Acidic Media. *ACS Appl. Energy Mater.* **2018**, *1*, 2849–2858.

(36) Liu, T.; Asiri, A. M.; Sun, X. Electrodeposited Co-Doped NiSe 2 Nanoparticles Film: A Good Electrocatalyst for Efficient Water Splitting. *Nanoscale* **2016**, *8*, 3911–3915.

(37) Carim, A. I.; Saadi, F. H.; Soriaga, M. P.; Lewis, N. S. Electrocatalysis of the Hydrogen-Evolution Reaction by Electrodeposited Amorphous Cobalt Selenide Films. *J. Mater. Chem. A* **2014**, *2*, 13835–13839.

(38) Zhang, H.; Yang, B.; Wu, X.; Li, Z.; Lei, L.; Zhang, X. Polymorphic CoSe 2 with Mixed Orthorhombic and Cubic Phases for Highly Efficient Hydrogen Evolution Reaction. *ACS Appl. Mater. Interfaces* **2015**, *7*, 1772–1779.

(39) Chhetri, M.; Sultan, S.; Rao, C. N. R. Electrocatalytic Hydrogen Evolution Reaction Activity Comparable to Platinum Exhibited by the Ni/Ni(OH) 2 /Graphite Electrode. *Proc. Natl. Acad. Sci.* **2017**, *114*, 8986–8990.

(40) Cao, M.; Xue, Z.; Niu, J.; Qin, J.; Sawangphruk, M.; Zhang, X.; Liu, R. Facile Electrodeposition of Ni–Cu–P Dendrite Nanotube Films with Enhanced Hydrogen Evolution Reaction Activity and Durability. *ACS Appl. Mater. Interfaces* **2018**, *10*, 35224–35233.

(41) Lu, X. F.; Yu, L.; Lou, X. W. (David). Highly Crystalline Ni-Doped FeP/Carbon Hollow Nanorods as All-PH Efficient and Durable Hydrogen Evolving Electrocatalysts. *Sci. Adv.* **2019**, *5*, eaav6009.

(42) Pu, Z.; Tang, C.; Luo, Y. Ferric Phosphide Nanoparticles Film Supported on Titanium Plate: A High-Performance Hydrogen Evolution Cathode in Both Acidic and Neutral Solutions. *Int. J. Hydrogen Energy* **2015**, *40*, 5092–5098.

(43) Sun, Y.; Liu, C.; Grauer, D. C.; Yano, J.; Long, J. R.; Yang, P.; Chang, C. J. Electrodeposited Cobalt-Sulfide Catalyst for Electrochemical and Photoelectrochemical Hydrogen Generation from Water. *J. Am. Chem. Soc.* **2013**, *135*, 17699–17702.

(44) Jiang, N.; You, B.; Sheng, M.; Sun, Y. Electrodeposited Cobalt-Phosphorous-Derived Films as Competent Bifunctional Catalysts for Overall Water Splitting. *Angew. Chem. Int. Ed.* **2015**, *54*, 6251–6254.

(45) Popczun, E. J.; Read, C. G.; Roske, C. W.; Lewis, N. S.; Schaak, R. E. Highly Active Electrocatalysis of the Hydrogen Evolution Reaction by Cobalt Phosphide Nanoparticles. *Angew. Chem. Int. Ed.* **2014**, *53*, 5427–5430.

(46) Pu, Z.; Luo, Y.; Asiri, A. M.; Sun, X. Efficient Electrochemical Water Splitting Catalyzed by Electrodeposited Nickel Diselenide Nanoparticles Based Film. *ACS Appl. Mater. Interfaces* **2016**, *8*, 4718–4723.

(47) Pei, Y.; Yang, Y.; Zhang, F.; Dong, P.; Baines, R.; Ge, Y.; Chu, H.; Ajayan, P. M.; Shen, J.; Ye, M. Controlled Electrodeposition Synthesis of Co–Ni–P Film as a Flexible and Inexpensive Electrode for Efficient Overall Water Splitting. *ACS Appl. Mater. Interfaces* **2017**, *9*, 31887–31896.

(48) Zhang, P.; Chen, H.; Wang, M.; Yang, Y.; Jiang, J.; Zhang, B.; Duan, L.; Daniel, Q.; Li, F.; Sun, L. Gas-Templating of Hierarchically Structured Ni–Co–P for Efficient Electrocatalytic Hydrogen Evolution. *J. Mater. Chem. A* **2017**, *5*, 7564–7570.

(49) Kim, H.; Oh, S.; Cho, E.; Kwon, H. 3D Porous Cobalt–Iron–Phosphorus Bifunctional Electrocatalyst for the Oxygen and Hydrogen Evolution Reactions. *ACS Sustain. Chem. Eng.* **2018**, *6*, 6305–6311.

(50) Popczun, E. J.; McKone, J. R.; Read, C. G.; Biacchi, A. J.; Wiltrout, A. M.; Lewis, N. S.; Schaak, R. E. Nanostructured Nickel Phosphide as an Electrocatalyst for the Hydrogen Evolution Reaction. *J. Am. Chem. Soc.* **2013**, *135*, 9267–9270.

(51) Li, D.; Batchelor-McAuley, C.; Compton, R. G. Some Thoughts about Reporting the Electrocatalytic Performance of Nanomaterials. *Appl. Mater. Today* **2020,** *18*, 100404.

(52) Zhang, Y.; Gao, L.; Hensen, E. J. M.; Hofmann, J. P. Evaluating the Stability of Co2P Electrocatalysts in the Hydrogen Evolution Reaction for Both Acidic and Alkaline Electrolytes. *ACS Energy Lett.* **2018**, *3*, 1360–1365.

(53) Wasalathanthri, R. N.; Jeffrey, S.; Awni, R. A.; Sun, K.; Giolando, D. M. Electrodeposited Copper–Cobalt–Phosphide: A Stable Bifunctional Catalyst for Both Hydrogen and Oxygen Evolution Reactions. *ACS Sustain. Chem. Eng.* **2019**, *7*, 3092–3100.

(54) Irshad, A.; Munichandraiah, N. Electrodeposited Nickel–Cobalt–Sulfide Catalyst for the Hydrogen Evolution Reaction. *ACS Appl. Mater. Interfaces* **2017**, *9*, 19746–19755.

(55) Chen, M.; Qi, J.; Zhang, W.; Cao, R. Electrosynthesis of NiPx nanospheres for Electrocatalytic Hydrogen Evolution from a Neutral Aqueous Solution. *Chem. Commun.* **2017**, *53*, 5507–5510.

(56) Zhang, L.; Liu, P. F.; Li, Y. H.; Wang, C. W.; Zu, M. Y.; Fu, H. Q.; Yang, X. H.; Yang, H. G. Accelerating Neutral Hydrogen Evolution with Tungsten Modulated Amorphous Metal Hydroxides. *ACS Catal.* **2018**, *8*, 5200–5205.

(57) Yoon, S.; Kim, J.; Lim, J.-H.; Yoo, B. Cobalt Iron-Phosphorus Synthesized by Electrodeposition as Highly Active and Stable Bifunctional Catalyst for Full Water Splitting. *J. Electrochem. Soc.* **2018**, *165*, H271–H276.

(58) Sun, C.; Zeng, J.; Lei, H.; Yang, W.; Zhang, Q. Direct Electrodeposition of Phosphorus-Doped Nickel Superstructures from Choline Chloride–Ethylene Glycol Deep Eutectic Solvent for Enhanced Hydrogen Evolution Catalysis. *ACS Sustain. Chem. Eng.* **2019**, *7*, 1529–1537.

(59) Jiang, N.; Bogoev, L.; Popova, M.; Gul, S.; Yano, J.; Sun, Y. Electrodeposited Nickel-Sulfide Films as Competent Hydrogen Evolution Catalysts in Neutral Water. *J. Mater. Chem. A* **2014**, *2*, 19407–19414.

(60) Liu, M.; Li, J. Cobalt Phosphide Hollow Polyhedron as Efficient Bifunctional Electrocatalysts for the Evolution Reaction of Hydrogen and Oxygen. *ACS Appl. Mater. Interfaces* **2016**, *8*, 2158–2165.

(61) Jiang, N.; You, B.; Sheng, M.; Sun, Y. Bifunctionality and Mechanism of Electrodeposited Nickel-Phosphorous Films for Efficient Overall Water Splitting. *ChemCatChem* **2016**, *8*, 106–112.